ACS OMEGA

http://pubs.acs.org/journal/acsodf

Article

Modified Beaded Materials from Recycled Wastes of Bagasse and Bagasse Fly Ash with Iron(III) Oxide-Hydroxide and Zinc Oxide for the Removal of Reactive Blue 4 Dye in Aqueous Solution

Pimploy Ngamsurach, Sutita Nemkhuntod, Pakdiporn Chanaphan, and Pornsawai Praipipat*

Cite This: *ACS Omega* 2022, 7, 34839−34857

Read Online

ACCESS | Metrics & More | Article Recommendations

ABSTRACT: Dye contamination in wastewater affects the photosynthesis of aquatic plants and algae by blocking the sunlight, and it induces toxicity to aquatic organisms, which might result in human health effects. Thus, the treatment of dyes in wastewater is required before discharging into the receiving water for safety purposes. Six dye adsorbent materials bagasse beads (BB), bagasse fly ash beads (BFB), bagasse beads with mixed iron(III) oxide-hydroxide (BBF), bagasse fly ash beads with mixed iron(III) oxide-hydroxide (BFBF), bagasse beads with mixed zinc oxide (BBZ), and bagasse fly ash beads with mixed zinc oxide (BFBZ) were synthesized and investigated using various characterization techniques such as X-ray diffractometry (XRD), field emission scanning electron microscopy with focused ion beam (FESEM-FIB), energy dispersive X-ray spectrometry (EDX), and Fourier transform infrared spectroscopy (FTIR). A series of batch experiments on the effects of dosage (0.5−3 g), contact time (3−18 h), temperature (30−80°C), pH (3−11), and initial concentration (30−90 mg/L) were used to investigate reactive blue 4 (RB4) dye removal efficiencies in aqueous solution, and their adsorption isotherms and kinetics were studied for explaining their adsorption patterns and mechanisms. All dye adsorbent materials demonstrated semicrystalline structures, and their surface morphologies had a spherical shape with coarse surfaces. Five main elements of oxygen, carbon, calcium, chlorine, and sodium and six main functional groups of alcohol and carboxylic acid (O−H), carbon dioxide (O═C═O), aromatic groups (C═O and N═O), alkene (C−H), and sodium alginate (C−O−C) were detected in all dye adsorbent materials. For batch tests, they could remove RB4 dye by more than 90%, and BFBF exhibited the highest RB4 dye removal efficiency at 99.36%. Freundlich and pseudo-second-order kinetic models well explained their adsorption patterns and mechanisms, in which BFBF demonstrated a higher maximum adsorption capacity (q_m) of 10.277 mg/g than that of other dye adsorbent materials. Therefore, all dye adsorbent materials offer good potential for further industrial applications.

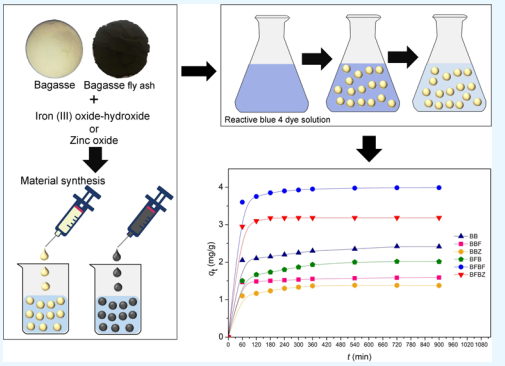

1. INTRODUCTION

Dye contaminants in the effluents of textile industries may create many environmental problems including blocking the sunlight and affecting the photosynthesis of aquatic plants and algae, and they are also toxic to aquatic organisms, accumulating through food web and resulting in human health effects such as allergy, dermatitis, skin irritation, and skin cancer.[1] Various dyes are widely used in many industries of pigments, paints, and textiles such as acid dyes, direct dyes, basic dyes, disperse dyes, reactive dyes, azoic dyes, etc.[2] Especially, reactive dyes are commonly used for dyeing cellulose fibers because of their long-lasting color; however, they are polyaromatic molecules, which make them more stable and cannot be biodegradable, resulting in environmental accumulations.[3] Therefore, the dye contaminant in wastewater is required to be treated before discharging to protect water bodies and the ecological system.

Coagulation−flocculation, ion exchange, advanced oxidation processes, reverse osmosis, photocatalytic degradation, phytoremediation, and adsorption are normally used for dye removal;[4] among them, adsorption is an effective method with easy operation and reasonable cost.[5] The selection of adsorbents is an challenge, as it has to provide high dye adsorption efficiency. Moreover, the cost−benefit management is also required for industrial applications, so low-cost adsorbents from waste materials might be a good choice to control the operation cost. Many research articles have used various waste materials such as sawdust, coconut shells, potato

Received: May 25, 2022
Accepted: September 9, 2022
Published: September 22, 2022

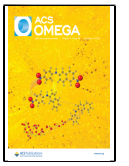

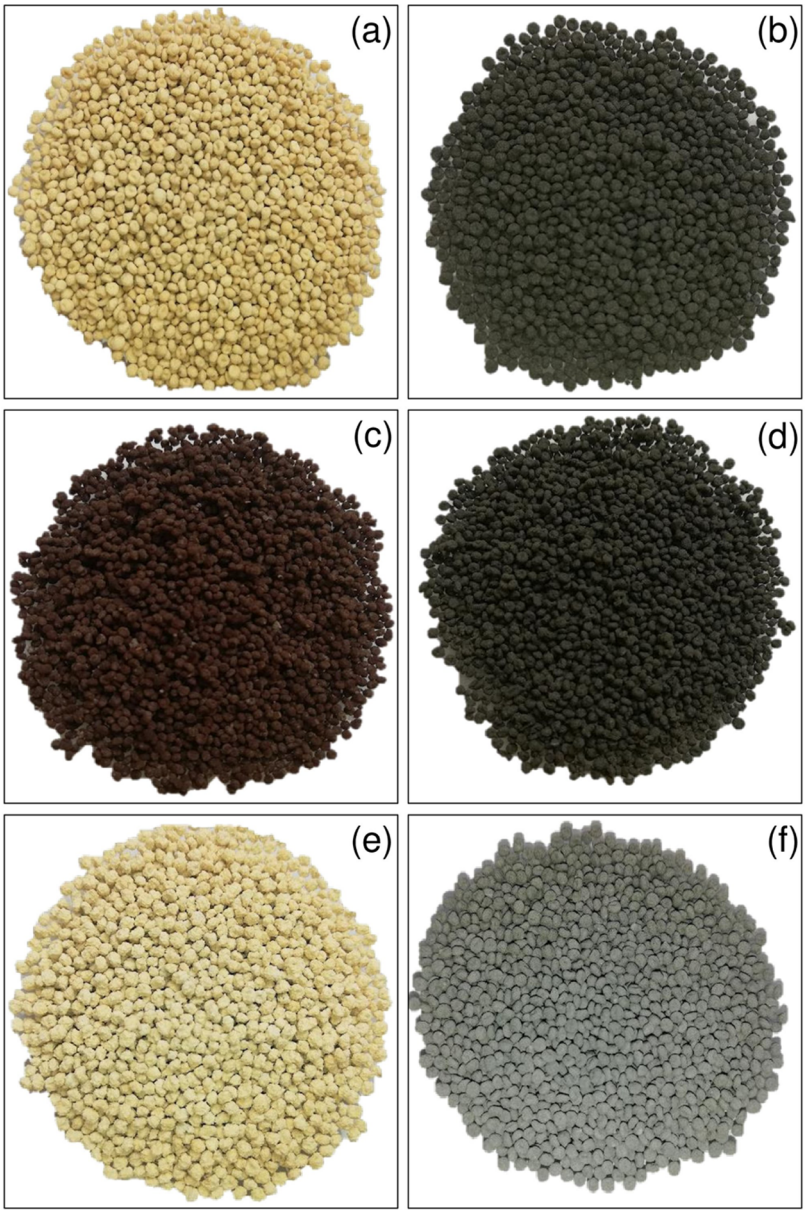

Figure 1. Physical characteristics of (a) bagasse beads (BB), (b) bagasse fly ash beads (BFB), (c) bagasse beads with mixed iron(III) oxide-hydroxide (BBF), (d) bagasse fly ash beads with mixed iron(III) oxide-hydroxide (BFBF), (e) bagasse beads with mixed zinc oxide (BBZ), and (f) bagasse fly ash beads with mixed zinc oxide (BFBZ).

peels, banana peels, rice husk, bagasse, and bagasse fly ash for dye removal in wastewater.[6−13] Among these, bagasse and bagasse fly ash are interesting choices because not only they have good chemical properties of cellulose, lignin, and hemicellulose for dye removal[14] but also they help reduce a huge amount of agriculture or industrial waste by acting as recycled waste for the wastewater treatment.

Many types of metal oxides such as titanium dioxide (TiO_2), aluminum oxide (Al_2O_3), manganese oxide (MnO), iron oxide (FeOH), and zinc oxide (ZnO) have been used for dye removal in various applications.[15] Especially, iron(III) oxide-hydroxide and ZnO are usually used for improving material efficiency to remove dyes in many articles.[16−19] Metal oxides are not appropriate for direct use in dye removal in effluents because they might cause problems including clogging, pressure drop, and being hard to separate after treatment.[20] Therefore, the adsorbent efficiencies are improved by adding them to raw materials. Also, changing the material form from powder to the beads might help solve the separation problem after treatment, which was proved and recommended by previous studies.[21,22] Therefore, this study attempts to synthesize dye adsorbent materials with the addition of metal oxides and changing the material form to improve dye adsorbent material efficiency for dye removal in wastewater for further industrial applications.

This current research attempted to synthesize six dye adsorbent materials such as bagasse beads (BB), bagasse fly ash beads (BFB), bagasse beads with mixed iron(III) oxide-hydroxide (BBF), bagasse fly ash beads with mixed iron(III) oxide-hydroxide (BFBF), bagasse beads with mixed zinc oxide (BBZ), and bagasse fly ash beads with mixed zinc oxide (BFBZ) for removal of the reactive blue 4 (RB4) dye in aqueous solution, to identify their characterizations with several techniques such as X-ray diffractometry (XRD), field

https://doi.org/10.1021/acsomega.2c03250
ACS Omega 2022, 7, 34839−34857

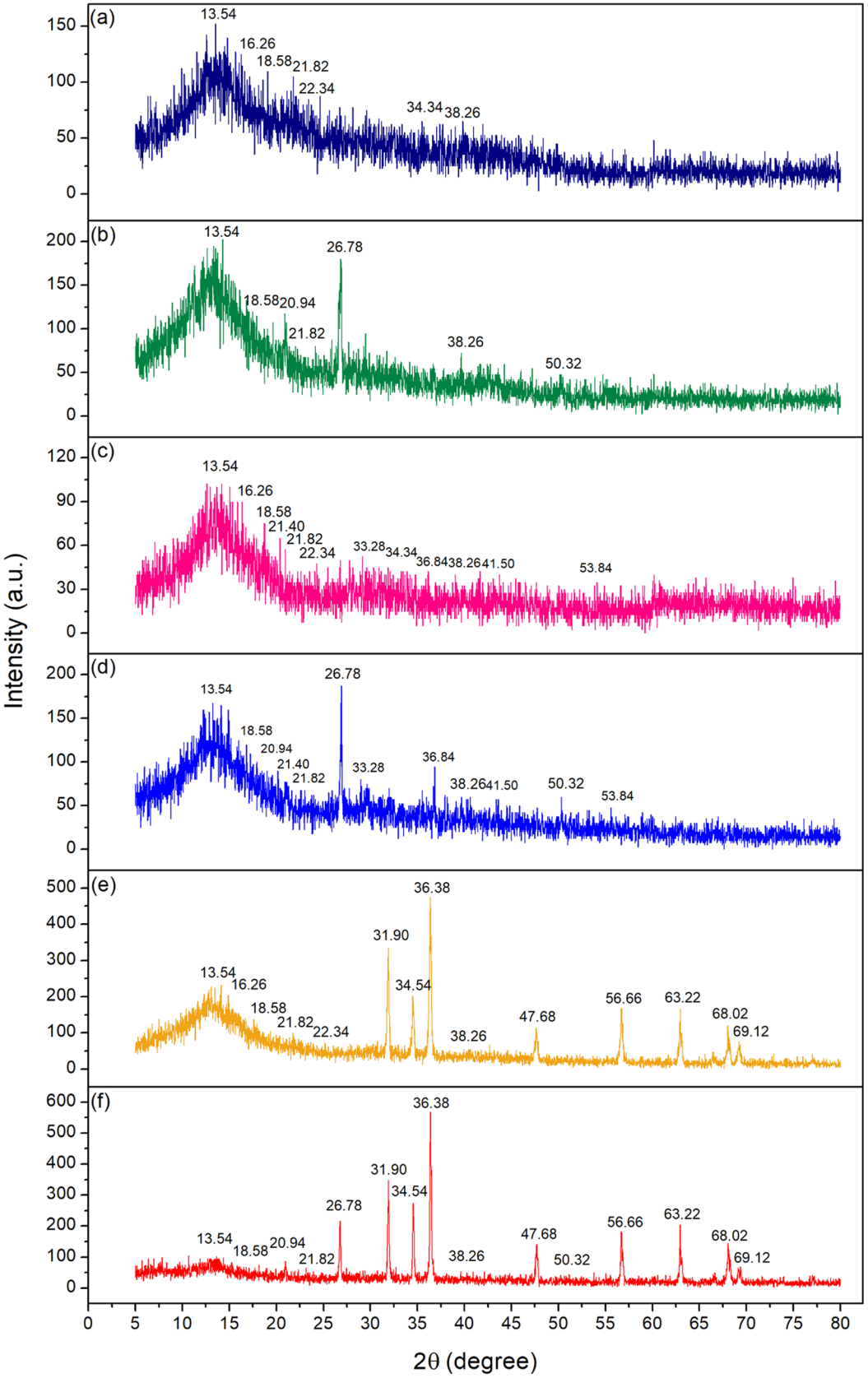

Figure 2. Crystalline structures of (a) bagasse beads (BB), (b) bagasse fly ash beads (BFB), (c) bagasse beads with mixed iron(III) oxide-hydroxide (BBF), (d) bagasse fly ash beads with mixed iron(III) oxide-hydroxide (BFBF), (e) bagasse beads with mixed zinc oxide (BBZ), and (f) bagasse fly ash beads with mixed zinc oxide (BFBZ).

https://doi.org/10.1021/acsomega.2c03250
ACS Omega 2022, 7, 34839−34857

emission scanning electron microscopy with focused ion beam (FESEM-FIB), energy dispersive X-ray spectrometry (EDX), and Fourier transform infrared spectroscopy (FTIR), to investigate their dye removal efficiencies with affecting factors such as dosage, contact time, temperature, pH, and initial concentration by a series of batch experiments and to study their adsorption isotherms and kinetics.

2. RESULTS AND DISCUSSION

2.1. Physical Characteristics of Dye Adsorbent Materials. Figure 1a−f demonstrates the physical characteristics of dye adsorbent materials, in which all materials had a spherical shape with different colors depending on the raw materials and types of metal oxides inside the materials. For BB and BFB, BB had a yellow color, whereas BFB had a dark-gray color, where their colors were directly correlated to the colors of bagasse and bagasse fly ash, respectively, as shown in Figure 1a,b. For BBF and BFBF, BBF had an iron-rust color, whereas BFBF had a black color, were the change of bead colors resulted from the addition of iron(III) oxide-hydroxide to the raw materials (BP and BFP) before synthesizing the bead materials, respectively, as shown in Figure 1c,d. For BBZ and BFBZ, BBZ had a light-yellow color, whereas BFBZ had a light-gray color, resulting from the addition of zinc oxide to the raw materials (BP and BFP), respectively, as shown in Figure 1e,f. The white color of zinc oxide has a decreasing effect on the colors of BBZ and BFBZ compared to the colors of BB and BFB.

2.2. Characterizations of Dye Adsorbent Materials. *2.2.1. XRD.* Figure 2a−f demonstrates the semicrystalline structures of all dye adsorbent materials using the XRD technique, and Table 1 illustrates their crystalline structures with their positions at 2θ (degree). BB and BFB demonstrated semicrystalline structures with specified cellulose structure peaks of 16.62, 22.34, and 34.34° for BB and specified SiO_2 peaks of 20.94, 26.78, and 50.32° for BFB, as shown in Figure 2a,b, respectively.[11,23] Moreover, it was also found that the specified sodium alginate peaks of 13.54, 18.58, 21.82, and 38.26° resulted from bead formations.[24] BBF and BFBF not only exhibited the specified peaks similarly to BB and BFB but also displayed the specified iron(III) oxide-hydroxide peaks of 21.40, 33.28, 36.84, 41.50, and 53.84° related to JCPDS:29-0713,[25] resulted from adding iron(III) oxide-hydroxide to BP and BFP before synthesizing bead materials, shown in Figure 2c,d, respectively. BBZ and BFBZ had the specified peaks similarly to BB and BFB, and they also had specified zinc oxide peaks of 31.90, 34.54, 36.38, 47.68, 56.66, 63.22, 68.02, and 69.12°, matching JCPDS:36-1451,[26] resulted from adding zinc oxide to BP and BFP before bead formation, as shown in Figure 2e,f, respectively. As a result, the successful addition of iron(III) oxide-hydroxide and zinc oxide to BP and BFP to synthesize BBF, BFBF, BBZ, and BFBZ could be confirmed.

2.2.2. FESEM-FIB and EDX. FESEM-FIB images of surface morphologies of dye adsorbent materials in the bead form at 100× magnification with 1 mm and the surface at 500× magnification with 400 μm are given in Figure 3a−l. BB and BFB had a spherical shape with coarse surfaces at 100× magnification with 1 mm, as shown in Figure 3a,c, respectively. At 500× magnification with 400 μm, the surface of BB displayed the layer sheet or scaly sheet surface, whereas BFB had a coarse surface, as shown in Figure 3b,d, respectively. BBF and BFBF had a spherical shape with coarse surfaces, among which BFBF presented a smoother surface than BBF at 100×

Table 1. Crystalline Structures of Bagasse Beads (BB), Bagasse Fly Ash Beads (BFB), Bagasse Beads with Mixed Iron(III) Oxide-Hydroxide (BBF), Bagasse Fly Ash Beads with Mixed Iron(III) Oxide-Hydroxide (BFBF), Bagasse Beads with Mixed Zinc Oxide (BBZ), and Bagasse Fly Ash Beads with Mixed Zinc Oxide (BFBZ) by XRD Analysis

	crystalline structures (2θ (degree))				
dye adsorbent materials	cellulose	SiO_2	sodium alginate	iron(III) oxide-hydroxide	zinc oxide
BB	16.62°, 22.34°, 34.34°		13.54°, 18.58°, 21.82°, 38.26°		
BFB		20.94°, 26.78°, 50.32°	13.54°, 18.58°, 21.82°, 38.26°		
BBF	16.62°, 22.34°, 34.34°		13.54°, 18.58°, 21.82°, 38.26°	21.40°, 33.28°, 36.84°, 41.50°, 53.84°	
BFBF		20.94°, 26.78°, 50.32°	13.54°, 18.58°, 21.82°, 38.26°	21.40°, 33.28°, 36.84°, 41.50°, 53.84°	
BBZ	16.62°, 22.34°, 34.34°		13.54°, 18.58°, 21.82°, 38.26°		31.90°, 34.54°, 36.38°, 47.68°, 56.66°, 63.22°, 68.02°, 69.12°
BFBZ		20.94°, 26.78°, 50.32°	13.54°, 18.58°, 21.82°, 38.26°		31.90°, 34.54°, 36.38°, 47.68°, 56.66°, 63.22°, 68.02°, 69.12°

https://doi.org/10.1021/acsomega.2c03250
ACS Omega 2022, 7, 34839−34857

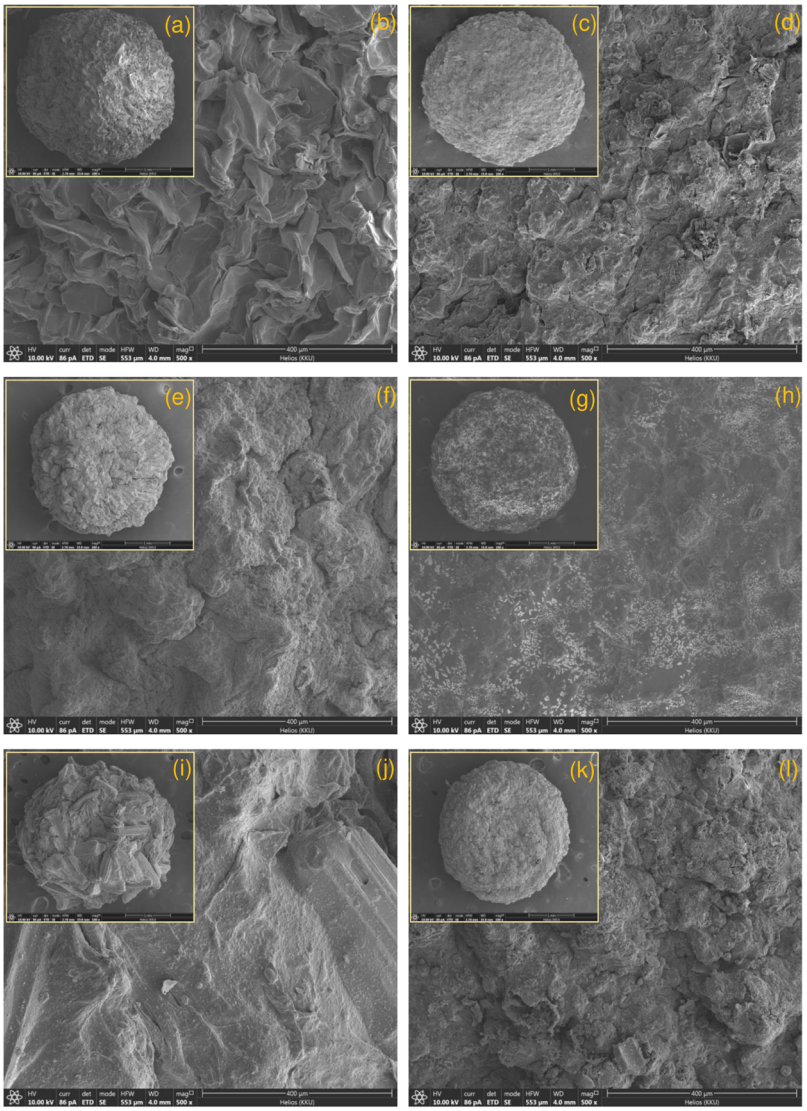

Figure 3. FESEM-FIB images of surface morphologies in the bead form at 100× magnification with 1 mm and surface at 500× magnification with 400 μm, respectively, of (a, b) bagasse beads (BB), (c, d) bagasse fly ash beads (BFB), (e, f) bagasse beads with mixed iron(III) oxide-hydroxide (BBF), (g, h) bagasse fly ash beads with mixed iron(III) oxide-hydroxide (BFBF), (i, j) bagasse beads with mixed zinc oxide (BBZ), and (k, l) bagasse fly ash beads with mixed zinc oxide (BFBZ).

Table 2. Average Chemical Compositions of Bagasse Beads (BB), Bagasse Fly Ash Beads (BFB), Bagasse Beads with Mixed Iron(III) Oxide-Hydroxide (BBF), Bagasse Fly Ash Beads with Mixed Iron(III) Oxide-Hydroxide (BFBF), Bagasse Beads with Mixed Zinc Oxide (BBZ), and Bagasse Fly Ash Beads with Mixed Zinc Oxide (BFBZ) by EDX Analysis

	chemical element (wt %)										
materials	O	C	Ca	Cl	Na	Fe	Zn	Si	Al	K	Mg
BB	43.9	43.6	8.1	3.8	0.6						
BBF	40.4	31.3	11.5	4.2	2.5	10.1					
BBZ	29.1	28.2	6.7	4.4	2.1		29.5				
BFB	31.4	38.6	12.6	3.9	0.8	1.3		9.2	1.5	0.4	0.3
BFBF	31.7	39.1	6.5	4.1	2.2	11.7		4.2	0.4	0.1	
BFBZ	20.5	30.3	5.7	4.1	1.2	2.3	30.4	4.5	0.7	0.3	

magnification with 1 mm, as shown in Figure 3e,g. At 500× magnification with 400 μm, BBF had a coarse surface, whereas BFBF had a smoother surface than BBF, as shown in Figure 3f,h. In addition, a little spreading of the iron rod in the surface of BFBF was also observed in Figure 3h. BBZ and BFBZ had a spherical shape with coarse surfaces, among which BFBZ showed a smoother surface than BBZ at 100× magnification with 1 mm, as shown in Figure 3I,k. At 500× magnification with 400 μm, both materials were also heterogeneous and has coarse surfaces, as shown in Figure 3j,l.

Table 2 demonstrates the average chemical compositions of all dye adsorbent materials by EDX analysis, which indicated the five main elements of oxygen (O), carbon (C), calcium (Ca), chlorine (Cl), and sodium (Na), whereas zinc (Zn) was

https://doi.org/10.1021/acsomega.2c03250
ACS Omega 2022, 7, 34839−34857

only detected in dye adsorbent materials with addition of ZnO. Iron (Fe) was found in dye adsorbent materials that consisted of bagasse fly ash as raw materials and dye adsorbent materials with addition of iron(III) oxide-hydroxide. Silicon (Si), aluminum (Al), and potassium (K) were only found in BFB, BFBF, and BFBZ, whereas magnesium (Mg) was only identified in BFB. For BB and BBF, O and C were decreased, whereas Ca, Cl, Na, and Fe were increased after addition of iron(III) oxide-hydroxide. As a result, this could verify the successful addition of Fe to bagasse powder (BP) before forming bead materials. For BB and BBZ, O, C, and Ca were decreased, whereas Cl, Na, and Zn were increased after addition of zinc oxide to confirm the addition of zinc oxide into bagasse powder (BP) before forming bead materials. For BFB and BFBF, O, C, Cl, Na, and Fe were increased, whereas Ca, Si, Al, K, and Mg were decreased after addition of iron(III) oxide-hydroxide. As a result, this could verify the addition of Fe to bagasse fly ash powder (BFP) before forming bead materials similarly to BBF. For BFB and BFBZ, O, C, Ca, Si, Al, K, and Mg were decreased, whereas Cl, Na, Fe, and Zn were increased after addition of zinc oxide to bagasse fly ash powder (BFP) before forming bead materials similarly to BBZ. Therefore, chemical compositions of all dye adsorbent materials were dependent on the raw materials and types of metal oxides that were added to the raw materials before forming bead materials.

2.2.3. FTIR. Figure 4a–f illustrates the chemical functional groups of all dye adsorbent materials by FTIR analysis, where

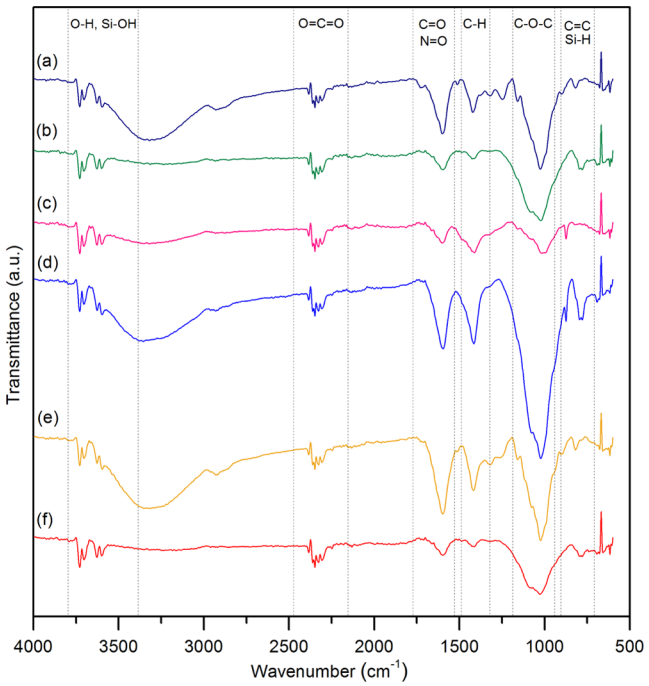

Figure 4. FTIR spectra of (a) bagasse beads (BB), (b) bagasse fly ash beads (BFB), (c) bagasse beads with mixed iron(III) oxide-hydroxide (BBF), (d) bagasse fly ash beads with mixed iron(III) oxide-hydroxide (BFBF), (e) bagasse beads with mixed zinc oxide (BBZ), and (f) bagasse fly ash beads with mixed zinc oxide (BFBZ).

the six main functional groups of O–H, O=C=O, C=O, N=O, C–H, and C–O–C were detected in all of them, and Table 3 demonstrates their functional groups with their positions by wavelength. O–H represents the stretching of alcohol and carboxylic acid, and O=C=O refers to the stretching of carbon dioxide.[27] C=O and N=O are the stretching of aromatic groups including carbonyl bonds of hemicellulose and the stretching of aromatic groups displaying lignin, respectively.[28,29] C–H represents the stretching of alkene, and C–O–C demonstrates the stretching of sodium alginate.[30] BB exhibited the stretching of O–H at 3737.93 and 3316.75 cm^{-1}, stretching of O=C=O at 2349.71 cm^{-1}, stretching of C=O and N=O at 1600.16 cm^{-1}, stretching of C–H at 1421.99 cm^{-1}, stretching of C–O–C at 1026.45 cm^{-1}, and stretching of C=C at 883.37 cm^{-1}, related to hemicellulose and cellulose in bagasse[31] shown in Figure 4a. BFB exhibited the stretching of O–H or Si–OH related to the silanol group at 3727.76, 3625.83, and 3600.45 cm^{-1}, stretching of O=C=O at 2349.66 cm^{-1}, stretching of C=O and N=O at 1596.13 cm^{-1}, stretching of C–H at 1424.74 cm^{-1}, stretching of C–O–C at 1019.17 cm^{-1}, and stretching of Si–H at 779.70 cm^{-1}, normally found in bagasse fly ash[27] shown in Figure 4b. BBF exhibited the stretching of O–H at 3727.86, 3703.37, 3626.30, 3599.89, and 3320.20 cm^{-1}, stretching of O=C=O at 2349.72 cm^{-1}, stretching of C=O and N=O at 1600.81 cm^{-1}, stretching of C–H at 1412.34 cm^{-1}, stretching of C–O–C at 1016.74 cm^{-1}, and stretching of C=C at 875.11 cm^{-1}, as shown in Figure 4c. BFBF demonstrated the stretching of O–H or Si–OH at 3728.29 and 3354.31 cm^{-1}, stretching of O=C=O at 2349.14 cm^{-1}, stretching of C=O and N=O at 1596.64 cm^{-1}, stretching of C–H at 1415.17 cm^{-1}, stretching of C–O–C at 1023.08 cm^{-1}, and stretching of Si–H at 779.38 cm^{-1}, as shown in Figure 4d. BBZ illustrated the stretching of O–H at 3727.70 and 3313.39 cm^{-1}, stretching of O=C=O at 2349.77 cm^{-1}, stretching of C=O and N=O at 1598.48 cm^{-1}, stretching of C–H at 1416.80 cm^{-1}, stretching of C–O–C at 1024.01 cm^{-1}, and stretching of C=C at 825.50 cm^{-1}, as shown in Figure 4e. BFBZ illustrated the stretching of O–H or Si–OH at 3728.10, 3626.51, and 3600.32 cm^{-1}, stretching of O=C=O at 2349.70 cm^{-1}, stretching of C=O and N=O at 1596.70 cm^{-1}, stretching of C–H at 1433.64 cm^{-1}, stretching of C–O–C at 1027.64 cm^{-1}, and stretching of Si–H at 779.60 cm^{-1}, as shown in Figure 4f.

2.3. Batch Experiments. *2.3.1. Effect of Dose.* Figure 5a was demonstrated the effect of dose from 0.5 to 3 g of dye adsorbent materials on dye removal efficiencies with the control condition of the initial dye concentration of 50 mg/L, a sample volume of 100 mL, a contact time of 12 h, pH 7, a temperature of 50 °C, and a shaking speed of 150 rpm. Dye removal efficiencies of all dye adsorbent materials were increased with the increasing of material dosage similarly to previous studies which the high amount of adsorbent dose contributed the high surface area and increased the adsorption sites for dye adsorption.[32] In this study, material dosages of 2, 3, 3, 2, 3, and 2 g demonstrated the highest dye removal efficiencies of 89.95, 90.80, 88.92, 92.34, 90.13, and 94.32% for BB, BFB, BBF, BFBF, BBZ, and BFBZ, respectively. Therefore, those material dosages were the optimum dosage of all dye adsorbent materials and used for studying of contact time effect.

2.3.2. Effect of Contact Time. Figure 5b was displayed the effect of contact time from 3 to 18 h of dye adsorbent materials on dye removal efficiencies with the control condition of the optimum dosage from 2.3.1, the initial dye concentration of 50 mg/L, a sample volume of 100 mL, pH 7, a temperature of 50 °C, and a shaking speed of 150 rpm. The trends of dye removal efficiencies of all dye adsorbent materials were increased with

https://doi.org/10.1021/acsomega.2c03250
ACS Omega 2022, 7, 34839–34857

Table 3. Functional Groups of Bagasse Beads (BB), Bagasse Fly Ash Beads (BFB), Bagasse Beads with Mixed Iron(III) Oxide-Hydroxide (BBF), Bagasse Fly Ash Beads with Mixed Iron(III) Oxide-Hydroxide (BFBF), Bagasse Beads with Mixed Zinc Oxide (BBZ), and Bagasse Fly Ash Beads with Mixed Zinc Oxide (BFBZ) by FTIR Analysis

	functional groups (wavenumber (cm^{-1}))						
dye adsorbent materials	O−H or Si−OH	O═C═O	C═O, N═O	C−H	C−O−C	C═C	Si−H
BB	3737.93, 3316.75	2349.71	1600.16	1421.99	1026.45	883.37	
BFB	3727.76, 3625.83, 3600.45	2349.66	1596.13	1424.74	1019.17		779.70
BBF	3727.86, 3703.37, 3626.30, 3599.89, 3320.20	2349.72	1600.81	1412.34	1016.74	875.11	
BFBF	3728.29, 3354.31	2349.14	1596.64	1415.17	1023.08		779.38
BBZ	3727.70, 3313.39	2349.77	1598.48	1416.80	1024.01	825.50	
BFBZ	3728.10, 3626.51, 3600.32	2349.70	1596.70	1433.64	1027.64		779.60

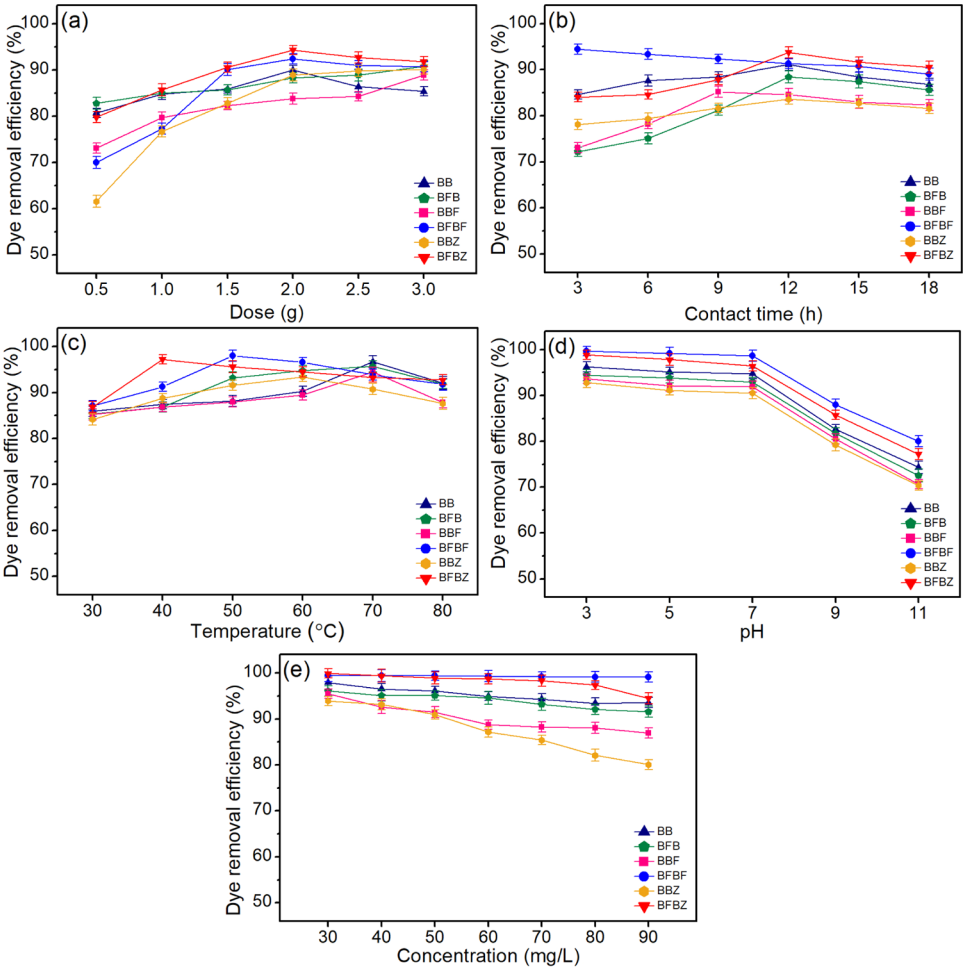

Figure 5. Batch experiments of bagasse beads (BB), bagasse fly ash beads (BFB), bagasse beads with mixed iron(III) oxide-hydroxide (BBF), bagasse fly ash beads with mixed iron(III) oxide-hydroxide (BFBF), bagasse beads with mixed zinc oxide (BBZ), and bagasse fly ash beads with mixed zinc oxide (BFBZ) in (a) dose, (b) contact time, (c) temperature, (d) pH, (e) concentration for dye adsorptions.

the increasing of contact time similarly to the results of effect of dose. Generally, the optimum contact time refers the time of the saturated dye adsorption on dye adsorbent, and dye adsorption will be constant or decrease after this time.[33] In this study, the highest dye removal efficiencies of almost dye adsorbent materials were found at 12 h with 91.09, 88.41, 83.56, and 93.78% for BB, BFB, BBZ, and BFBZ, respectively except BBF and BFBF which were found at 9 and 3 h with 85.21 and 94.44%. Therefore, those contact times were the optimum contact time of all dye adsorbent materials and used for studying of temperature effect.

2.3.3. Effect of Temperature. Figure 5c was displayed the effect of temperature from 30 to 80 °C of dye adsorbent materials on dye removal efficiencies with the control condition of the optimum dosage and contact time from 2.3.1 and 2.3.2, the initial dye concentration of 50 mg/L, a sample volume of 100 mL, pH 7, and a shaking speed of 150 rpm. The temperatures of 70, 70, 70, 50, 60, and 40 °C illustrated the highest dye removal efficiencies of 96.66, 95.64, 94.51, 97.98, 93.38, and 97.21% for BB, BFB, BBF, BFBF, BBZ, and BFBZ, respectively. After those temperatures, dye removal efficiencies of all dye adsorbent materials were decreased. Since the criteria of choosing the optimum

https://doi.org/10.1021/acsomega.2c03250
ACS Omega 2022, 7, 34839−34857

condition in this study was the lowest value of each parameter which it obtained the highest dye removal efficiency, those temperatures were used for studying of pH effect as the optimum temperatures of all dye adsorbent materials. However, the low temperature was recommended to be operation for safe natural environment after treatment. Since the dye removal efficiencies of all dye adsorbent materials were more than 85% in a range of temperatures of 30−50 °C, those temperature were good choices for applying in a real wastewater treatment operation.

2.3.4. Effect of pH. Figure 5d displays the effect of pH from 3 to 11 of dye adsorbent materials on dye removal efficiencies with the control conditions optimum dosage, contact time, and temperature from 2.3.1, 2.3.2, and 2.3.3, the initial dye concentration of 50 mg/L, a sample volume of 100 mL, and a shaking speed of 150 rpm. Dye removal efficiencies of all dye adsorbent materials were decreased with increasing pH values, among which pH 3 demonstrated the highest dye removal efficiencies of 96.23, 94.45, 93.62, 99.69, 92.78, and 98.88% for BB, BFB, BBF, BFBF, BBZ, and BFBZ, respectively. In addition, the point of zero charge (pH_{pzc}), which is a pH value at the net charge equal to zero, is generally used for considering which pH is optimal for good adsorption by the adsorbent.[34] As a result, this study investigated the point of zero charge of all dye adsorbent materials, as shown in Figure 6a,b. Figure 6a represents the results of pH_{pzc} of BB, BBF, and BBZ; their pH_{pzc} values were 7.13, 7.28, and 7.48, respectively. pH_{pzc} values of BFB, BFBF, and BFBZ were 7.25, 7.39, and 7.55, respectively, shown in Figure 6b. Addition of iron(III) oxide-hydroxide and zinc oxide increased the pH_{pzc} values of BB and BFB, and zinc oxide resulted in more increasing pH_{pzc} than iron(III) oxide-hydroxide. In the case of anionic dyes, the pH of the solution should be lower than pH_{pzc} because dye ions are well adsorbed by the positive charge of dye adsorbents. Therefore, the pH solution should be lower than pH 7 ($pH < pH_{pzc}$) to obtain high adsorption efficiencies by all dye adsorbent materials. Moreover, these results agreed with other studies that anionic dyes were highly adsorbed at low pH or acidic pH because of the electrostatic interactions on the positive surface charge of dye adsorbent materials.[35] In an opposite way, increasing pH values especially alkaline pHs increased the −OH or negative charge sites of dye adsorbent materials, so dye removal efficiencies were decreased. Therefore, pH 3 was the optimum pH of all dye adsorbent materials and used for characterizing the effect of concentration.

2.3.5. Effect of Concentration. Figure 5e displays the effect of concentration from 30 to 90 mg/L of dye adsorbent materials on dye removal efficiencies with the control conditions optimum dosage, contact time, temperature, and pH from 2.3.1, 2.3.2, 2.3.3, and 2.3.4, a sample volume of 100 mL, and a shaking speed of 150 rpm. Dye removal efficiencies from 30 to 90 mg/L of BB, BFB, BBF, BFBF, BBZ, and BFBZ were 93.56−97.91, 91.57−96.07, 86.92−95.49, 99.10−99.49, 80.05−93.88, and 94.51−99.86%, respectively; they were decreased with increasing dye concentration. These results corresponded to other studies that increasing initial dye concentration decreased active adsorbent sites and resulted in the decrease of dye removal efficiency.[36] For the dye concentration of 50 mg/L, dye removal efficiencies of BB, BFB, BBF, BFBF, BBZ, and BFBZ were 96.09, 95.08, 91.44, 99.36, 90.92, and 98.88%, respectively, and BFBF demonstrated the highest dye removal efficiency than others. Therefore, all dye adsorbent materials were high-quality

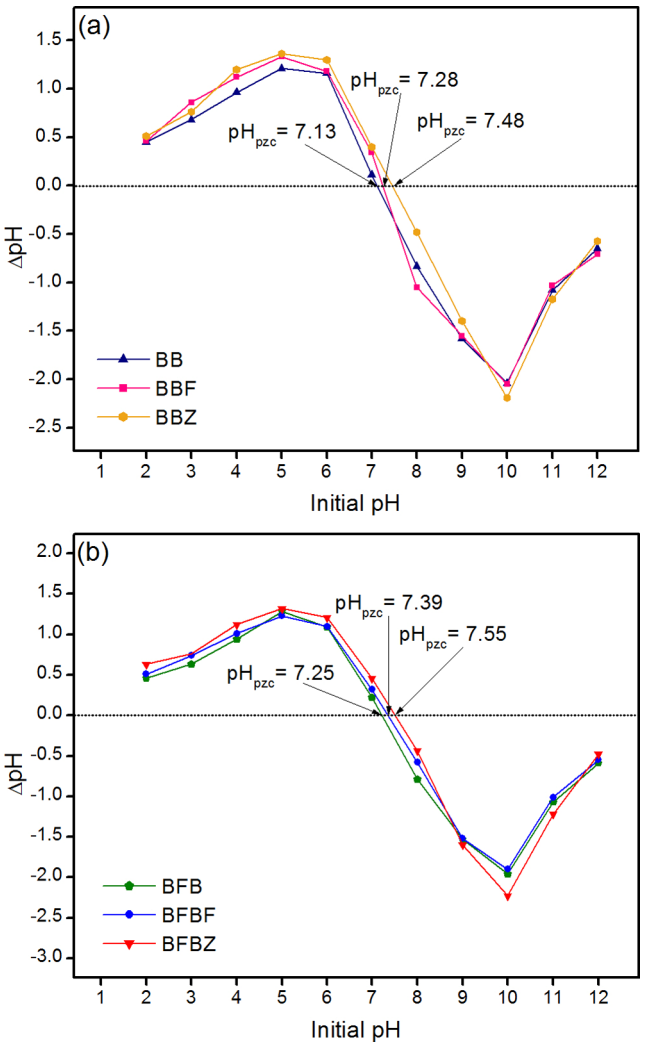

Figure 6. Point of zero charge of all dye adsorbent materials of (a) bagasse beads (BB), bagasse beads with mixed iron(III) oxide-hydroxide (BBF), and bagasse beads with mixed zinc oxide (BBZ) and (b) bagasse fly ash beads (BFB), bagasse fly ash beads with mixed iron(III) oxide-hydroxide (BFBF), and bagasse fly ash beads with mixed zinc oxide (BFBZ).

adsorbents for a dye removal of 50 mg/L in wastewater more than 90%.

In conclusion, 2 g, 12 h, 70 °C, pH 3, and 50 mg/L; 3 g, 12 h, 70 °C, pH 3, and 50 mg/L; 3 g, 9 h, 70 °C, pH 3, and 50 mg/L; 2 g, 3 h, 50 °C, pH 3, and 50 mg/L; 3 g, 12 h, 60 °C, pH 3, and 50 mg/L; and 2 g, 12 h, 40 °C, pH 3, and 50 mg/L were the optimum conditions in dosage, contact time, temperature, pH, and concentration of BB, BFB, BBF, BFBF, BBZ, and BFBZ, respectively, and they could be arranged in order from high to low as BFBF > BFBZ > BB > BFB > BBF > BBZ. From these results, BFBF and BFBZ spent less amounts of adsorbent, contact time, and temperature than BFB, and they exhibit higher dye removal efficiencies than that of BFB. Therefore, the addition of metal oxides to bagasse fly ash not only helped increase dye material efficiencies similarly to other studies[37,38] but also decreased the operation cost. As a result, only dye adsorbent materials using bagasse fly ash as a raw material with metal oxides could increase dye removal efficiencies, whereas dye adsorbent materials with bagasse without metal oxide (BB) demonstrated higher dye removal

https://doi.org/10.1021/acsomega.2c03250
ACS Omega 2022, 7, 34839−34857

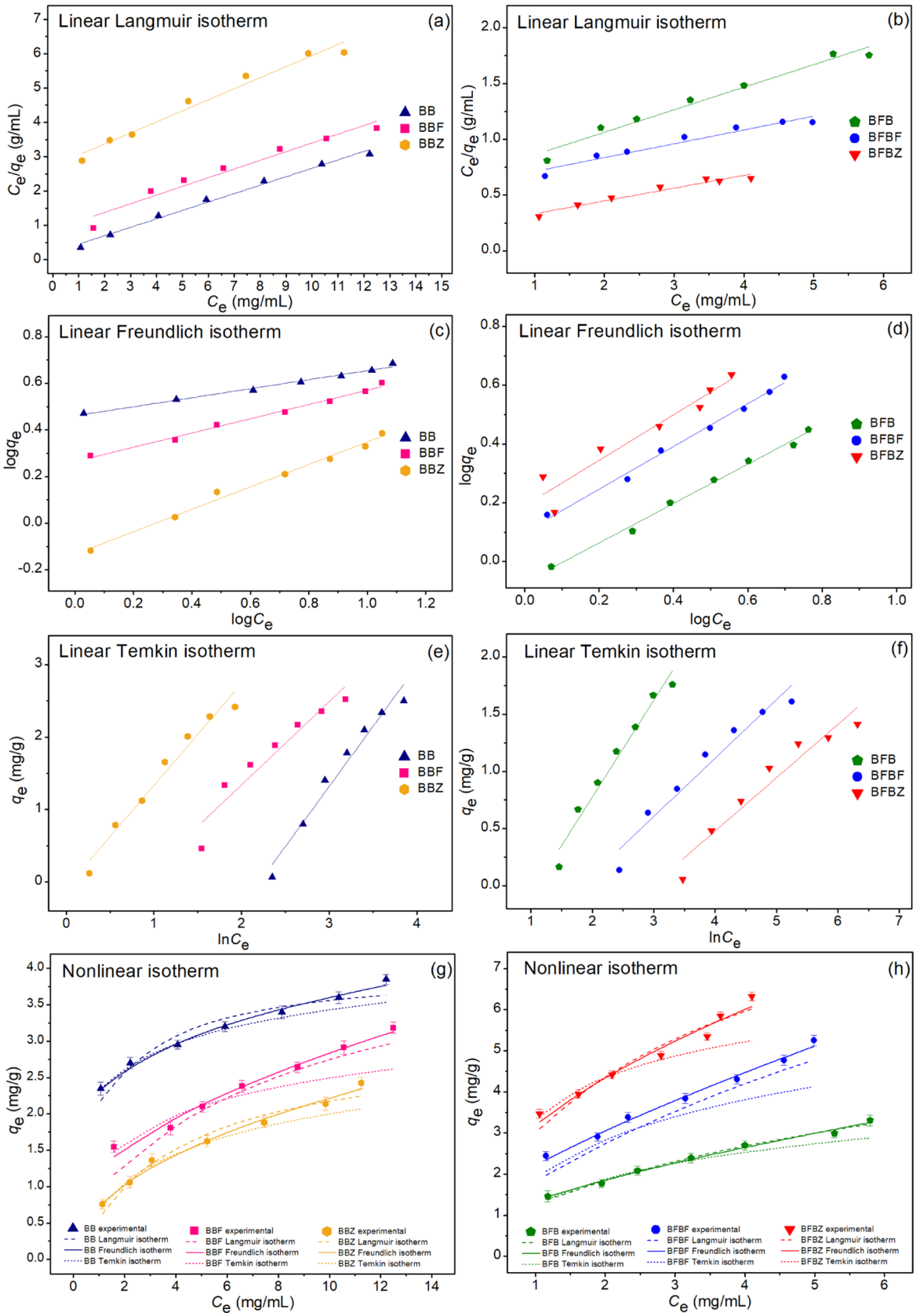

Figure 7. (a, b) linear Langmuir, (c, d) linear Freundlich, (e, f) linear Temkin, and (g, h) nonlinear adsorption isotherms of bagasse beads (BB), bagasse fly ash beads (BFB), bagasse beads with mixed iron(III) oxide-hydroxide (BBF), bagasse fly ash beads with mixed iron(III) oxide-hydroxide (BFBF), bagasse beads with mixed zinc oxide (BBZ), and bagasse fly ash beads with mixed zinc oxide (BFBZ) for dye adsorptions.

https://doi.org/10.1021/acsomega.2c03250
ACS Omega 2022, 7, 34839−34857

Table 4. Equilibrium Isotherm Parameters of Bagasse Beads (BB), Bagasse Fly Ash Beads (BFB), Bagasse Beads with Mixed Iron(III) Oxide-Hydroxide (BBF), Bagasse Fly Ash Beads with Mixed Iron(III) Oxide-Hydroxide (BFBF), Bagasse Beads with Mixed Zinc Oxide (BBZ), and Bagasse Fly Ash Beads with Mixed Zinc Oxide (BFBZ) for Dye Adsorptions

regression method	model	parameter	BB	BFB	BBF	BFBF	BBZ	BFBZ
linear	Langmuir	q_m (mg/g)	3.170	5.571	3.765	10.277	3.178	6.775
		K_L (L/mg)	0.175	0.162	0.148	0.129	0.307	0.383
		R^2	0.984	0.956	0.914	0.877	0.977	0.862
	Freundlich	$1/n$	0.297	0.671	0.500	0.727	0.418	0.565
		K_F (mg/g)(L/mg)$^{1/n}$	0.975	0.849	0.695	1.261	0.924	1.917
		R^2	0.994	0.994	0.969	0.992	0.991	0.972
	Temkin	b_T (J/mol)	4821.614	2481.041	3580.059	1017.138	4018.876	1793.682
		A_T (L/g)	2.900	1.713	1.575	1.164	3.123	3.936
		R^2	0.972	0.971	0.915	0.959	0.971	0.903
nonlinear	Langmuir	q_m (mg/g)	3.001	5.845	4.098	12.074	3.134	7.884
		K_L (L/mg)	0.216	0.150	0.122	0.102	0.315	0.288
		R^2	0.923	0.990	0.946	0.984	0.961	0.938
		R_{adj}^2	0.908	0.988	0.936	0.981	0.953	0.925
		RMSE	0.159	0.073	0.150	0.139	0.129	0.280
	Freundlich	$1/n$	0.303	0.667	0.552	0.756	0.418	0.628
		K_F (mg/g)(L/mg)$^{1/n}$	0.960	0.853	0.628	1.218	0.924	1.823
		R^2	0.991	0.992	0.983	0.991	0.989	0.966
		R_{adj}^2	0.990	0.991	0.980	0.989	0.987	0.960
		RMSE	0.054	0.064	0.084	0.105	0.069	0.206
	Temkin	b_T (J/mol)	5776.959	3088.967	5193.514	1916.943	4789.275	2616.058
		A_T (L/g)	5.102	2.266	3.156	2.309	4.505	7.255
		R^2	0.978	0.988	0.960	0.988	0.978	0.901
		R_{adj}^2	0.973	0.985	0.952	0.986	0.974	0.881
		RMSE	0.162	0.231	0.334	0.445	0.177	0.601

efficiency than that of dye adsorbent materials of bagasse with metal oxide (BBF and BBZ). Finally, BFBF demonstrated the highest dye removal efficiency than that of other dye adsorbent materials.

2.4. Isotherm Study. The adsorption patterns of dye adsorbent materials were identified by plotting linear and nonlinear models of Langmuir, Freundlich, and Temkin isotherms. For linear models, Langmuir, Freundlich, and Temkin isotherms were plotted by C_e/q_e versus C_e, $\log q_e$ versus $\log C_e$, and q_e versus $\ln C_e$, respectively. For nonlinear models, all isotherms were plotted by C_e versus q_e. Figure 7a–h demonstrates the plotting results of all isotherm models, and Table 4 illustrates their equilibrium isotherm parameters.

The regression value (R^2) is generally used to characterize which isotherm model well explains the adsorption pattern of the adsorbent material. A higher R^2 is preferred especially closely to 1.[21,22] Since the R^2 values of BB, BFB, BBF, BFBF, BBZ, and BFBZ in both linear and nonlinear Freundlich models were higher than those of Langmuir and Temkin models, their adsorption patterns corresponded to the Freundlich isotherm in relation to physicochemical adsorption.[39] Therefore, Freundlich parameters of K_F and $1/n$ values were used for explaining the adsorption pattern. K_F refers to the Freundlich adsorption constant;[21,40] BFBZ exhibited the highest K_F value than that of other adsorbents. The $1/n$ value is a constant depicting the adsorption intensity, where $0 < 1/n < 1$ means the favorable adsorption isotherm, and higher $1/n$ represents high equilibrium adsorption capacity.[21,40] Therefore, BFBF demonstrated the highest equilibrium adsorption capacity than that of other dye adsorbent materials correlated to the results of batch experiments. Moreover, since the equilibrium parameters and R^2 of BB, BFB, BBF, BFBF, BBZ, and BFBZ on dye adsorptions by linear and nonlinear Langmuir, Freundlich, and Temkin isotherm models had approximately closer values; their results were consistent with each other. Therefore, both linear and nonlinear isotherm models were required to plot graphs for preventing data mistranslation.[22,41]

Finally, the comparison of the maximum dye adsorption capacity (q_m) of this study with that of other adsorbents for reactive blue 4 (RB4) dye removal is represented in Table 5. Almost all adsorbents had a higher q_m value in this study except pecan nut shells[42] and chitosan glutaraldehyde-cross-linked beads.[39] Different conditions such as raw materials, adsorbent dose, contact time, pH, and initial concentration of all adsorbents might affect the different q_m values, which could not be directly compared with each other including this study. Although all dye adsorbent materials in this study had lower q_m values than others, they demonstrated higher RB4 dye removal efficiencies more than 90%, which could guarantee the available active sites of all dye adsorbent materials.

2.5. Kinetic Study. Linear and nonlinear kinetic models of the pseudo-first order, pseudo-second order, and intraparticle diffusion were used to explain the adsorption rate and mechanism of dye adsorbent materials. For linear models, the pseudo-first-order kinetic model, pseudo-second-order kinetic model, and intraparticle diffusion model were plotted by $\ln(q_e - q_t)$ versus time (t), t/q_t versus time (t), and q_t versus time ($t^{0.5}$), respectively. For nonlinear models, the pseudo-first-order and pseudo-second-order kinetic models were plotted by q_t versus time (t). Figure 8a–h demonstrates the plotting results of all kinetic models, and Table 6 illustrates their adsorption kinetic parameters.

The best-fitted model of the adsorption mechanism is chosen using the same criteria of adsorption isotherms that a higher R^2 value or that close to 1 is selected. Since the R^2

https://doi.org/10.1021/acsomega.2c03250
ACS Omega 2022, 7, 34839−34857

Table 5. Comparison of the Maximum Dye Adsorption Capacity (q_m) with Various Adsorbents for Reactive Blue 4 (RB4) Dye Removal

adsorbents	q_m (mg/g)	references
bagasse (modified propionic acid)	13.20	32
mustard stalk activated carbon	25.80	43
bokbunja waste seeds untreated with *n*-hexane	25.44	44
bokbunja waste seeds treated with *n*-hexane	26.16	44
surfactant modified barley straw	29.16	45
pecan nut shells	7.91	42
peanut shell modified with IL	30.20	46
peanut shell-activated carbon modified with IL	376.25	46
rice bran (modified with magnetite)	181.82	47
rice bran (modified with SnO_2/Fe_3O_4)	217.39	48
calcium alginate immobilized cells	15.87	49
calcium alginate immobilized EPS	18.65	49
extracellular polymeric substances	42.93	49
dry cells of *Rhizopus oryzae* biomass	101.10	50
activated carbon developed from *Enteromorpha prolifera*	131.93	51
lanthanum incorporated carboxymethylcellulose-bentonite composite	45.87	33
polymetallic nanoparticles from spent lithium-ion batteries	345.00	52
guar gum and silica nanocomposite	579.01	53
chitosan glutaraldehyde-crosslinked beads	1.76	39
chitosan@hydroxyapatite nanocomposite	166.80	54
chitosan activated charcoal composite (modified Fe_3O_4)	250.00	55
chitosan	200.00	56
chitosan modified with HAD/APTES beads	666.70	56
BB	3.17	this study
BFB	5.57	this study
BBF	3.77	this study
BFBF	10.28	this study
BBZ	3.18	this study
BFBZ	6.78	this study

values of BB, BFB, BBF, BFBF, BBZ, and BFBZ in both linear and nonlinear pseudo-second-order kinetic models were higher than those of pseudo-first-order kinetic and intraparticle diffusion models, their adsorption rate and mechanism of all dye adsorbent materials corresponded to the pseudo-second-order kinetic model with relation to the chemisorption process with heterogeneous adoption, similar to that reported in other studies.[42,50,52] Therefore, the adsorption kinetic parameters of q_e and k_2 were used for explaining the adsorption mechanism. The adsorption capacity (q_e) of the pseudo-first-order kinetic model in the order from high to low was BFBF > BFBZ > BB > BFB > BBF > BBZ, correlating with the results of batch experiments and adsorption isotherms. The k_2 value is the pseudo-second-order kinetic rate constant of which BFBF demonstrated the highest value than that of other adsorbents. Finally, the results of both linear and nonlinear pseudo-first-order, pseudo-second-order kinetic, and intraparticle models of all dye adsorbent materials were consistent to each other, so the plotting of both linear and nonlinear kinetic models was also recommended for correct data translations.[22,41]

2.6. Possible Mechanism of RB4 Dye Adsorption by Dye Adsorbent Materials. The possible mechanism of RB4 dye adsorption by dye adsorbent materials (BB, BFB, BBF, BFBF, BBZ, and BFBZ) is demonstrated in Figure 9. The surfaces of all dye adsorbent materials had the main functional groups of O−H, O═C═O, C═O, N═O, C−H, and C−O−C reported by FTIR. BBF, BFBF, BBZ, and BFBZ also exhibited the complex molecules of Fe-$(OH)_3$ or ZnO with hydroxyl groups (−OH) through sharing electrons.[57] The main mechanism of RB4 dye adsorption on dye adsorbent materials might contain three possible reactions, which were electrostatic attractions, hydrogen bonding interactions, and n−π bonding interactions.[39] For electrostatic interactions, RB4 dye molecules with negatively charged sulfonate groups ($-SO_3^-$) interacted with the positively charged hydroxy group (−OH) on the surfaces of dye adsorbent materials at acid pH (pH < pH_{pzc}),[58] their pH_{pzc} values are reported in Figure 6. For hydrogen bonding interactions, the hydrogen ions (H^+) of the hydroxyl group (−OH) in dye adsorbent materials reacted with the nitrogen (N) of the dye molecule for RB4 dye removal.[59] Finally, the hydroxyl group (−OH) or oxygen bond (−O) in dye adsorbent materials reacted with the aromatic rings of RB4 dye molecules for facilitating n−π bonding interactions.[60]

3. CONCLUSIONS

Six dye adsorbent materials such as bagasse beads (BB), bagasse fly ash beads (BFB), bagasse beads with mixed iron(III) oxide-hydroxide (BBF), bagasse fly ash beads with mixed iron(III) oxide-hydroxide (BFBF), bagasse beads with mixed zinc oxide (BBZ), and bagasse fly ash beads with mixed zinc oxide (BFBZ) were synthesized for the removal of reactive blue 4 (RB4) dye in aqueous solution. All materials had a spherical shape with different colors dependent upon the colors of raw materials and metal oxides. All dye adsorbent materials demonstrated semicrystalline structures with specific peaks of sodium alginate, and the specified peaks of iron(III) oxide-hydroxide and zinc oxide were found in BBF, BFBF, BBZ, and BFBZ. Their surface morphologies had spherical shapes with coarse surfaces, and five main elements of oxygen (O), carbon (C), calcium (Ca), chlorine (Cl), and sodium (Na) were found in all dye adsorbent materials. Six main functional groups of O−H, O═C═O, C═O, N═O, C−H, and C−O−C were detected in all materials. The optimum conditions of BB, BFB, BBF, BFBF, BBZ, and BFBZ for RB4 dye adsorption of 50 mg/L were 2 g, 12 h, 70 °C, and pH 3; 3 g, 12 h, 70 °C, and pH 3; 3 g, 9 h, 70 °C, and pH 3; 2 g, 3 h, 50 °C, and pH 3; 3 g, 12 h, 60 °C, and pH 3; and 2 g, 12 h, 40 °C, and pH 3, respectively, and they could be arranged in order from high to low as BFBF > BFBZ > BB > BFB > BBF > BBZ, which could remove RB4 dye more than 90%. As a result, both the change of the material form and addition of metal oxide helped improve dye adsorbent efficiencies. Especially, dye materials from bagasse fly ash with iron(III) oxide-hydroxide represented the highest RB4 dye removal in this study. For adsorption isotherms and kinetics, they corresponded to the Freundlich model and pseudo-second-order kinetic models with relation to the physicochemical adsorption and chemosorption process. Therefore, all dye adsorbent materials are potential materials for RB4 dye adsorptions in aqueous solution, and they might be used for industrial applications in the future. For future studies, the possible reuse of materials needs to be investigated through the desorption experiments, and the continuous flow study is also required for real industrial wastewater treatment applications.

https://doi.org/10.1021/acsomega.2c03250
ACS Omega 2022, 7, 34839−34857

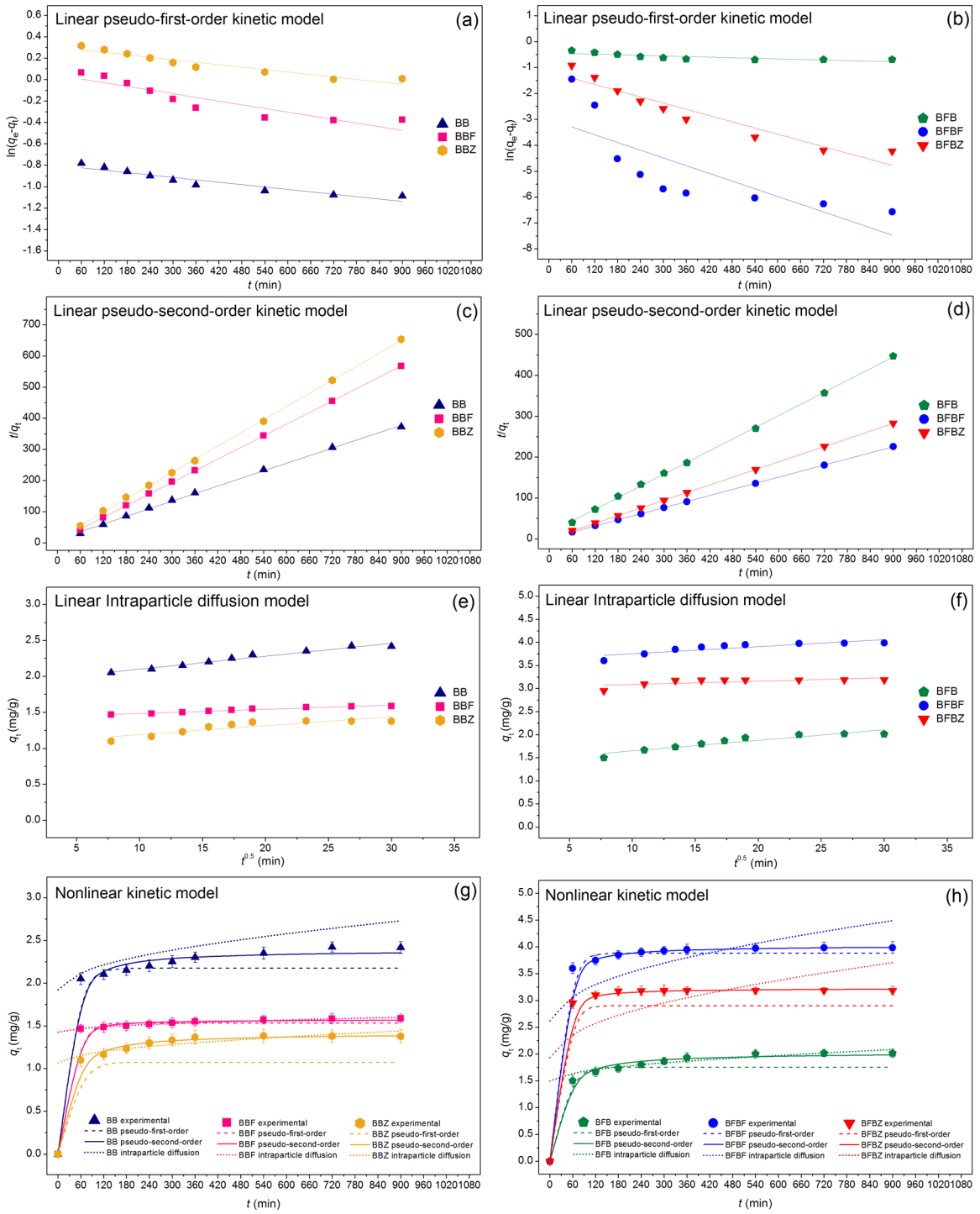

Figure 8. (a and b) linear pseudo-first-order, (c and d) linear pseudo-second-order, (e and f) linear intraparticle diffusion, and (g and h) nonlinear kinetic models of bagasse beads (BB), bagasse fly ash beads (BFB), bagasse beads with mixed iron(III) oxide-hydroxide (BBF), bagasse fly ash beads with mixed iron(III) oxide-hydroxide (BFBF), bagasse beads with mixed zinc oxide (BBZ), and bagasse fly ash beads with mixed zinc oxide (BFBZ) for dye adsorptions.

4. MATERIALS AND METHODS

4.1. Raw Materials. Bagasse was collected from a local market in Khon Kaen province, Thailand, and bagasse fly ash was collected from a sugar factory in Khon Kaen province, Thailand.

4.2. Raw Material Preparations. Bagasse was washed using tap water to eliminate contamination, and then, it was dried overnight using a hot air oven (Binder, FED 53, Germany) at 80 °C. After that, it was ground and sieved to a size of 125 μm, and it was kept in a desiccator before use, called bagasse powder (BP). Bagasse fly ash was sieved to a size of 125 μm, and then, it was kept in a desiccator before use, called bagasse fly ash powder (BFP).

4.3. Chemicals. All chemicals were analytical grade (AR) and used without purification. For modified bead materials, ferric chloride hexahydrate ($FeCl_3{\cdot}6H_2O$) (LOBA, India),

https://doi.org/10.1021/acsomega.2c03250
ACS Omega 2022, 7, 34839−34857

Table 6. Adsorption Kinetic Parameters of Bagasse Beads (BB), Bagasse Fly Ash Beads (BFB), Bagasse Beads with Mixed Iron(III) Oxide-Hydroxide (BBF), Bagasse Fly Ash Beads with Mixed Iron(III) Oxide-Hydroxide (BFBF), Bagasse Beads with Mixed Zinc Oxide (BBZ), and Bagasse Fly Ash Beads with Mixed Zinc Oxide (BFBZ) for Dye Adsorptions

regression method	model	parameter	BB	BFB	BBF	BFBF	BBZ	BFBZ
linear	pseudo-first-order kinetic model	q_e (mg/g)	1.352	1.039	0.870	0.050	0.449	0.311
		k_1 (min^{-1})	0.0004	0.0006	0.0004	0.0050	0.0004	0.0040
		R^2	0.915	0.847	0.656	0.625	0.905	0.914
	pseudo-second-order kinetic model	q_e (mg/g)	2.277	1.592	1.417	2.597	1.304	2.526
		k_2 (g/mg·min)	0.0164	0.0149	0.0348	0.1215	0.0558	0.0312
		R^2	0.999	0.999	1.000	0.952	1.000	1.000
	intraparticle diffusion	k_i (mg/g·$min^{0.5}$)	0.0179	0.0196	0.0125	0.0072	0.0058	0.0153
		C_i (mg/g)	1.722	0.995	1.065	2.316	1.126	2.102
		R^2	0.967	0.915	0.783	0.454	0.962	0.748
nonlinear	pseudo-first-order kinetic model	q_e (mg/g)	1.459	1.122	0.939	0.054	0.484	0.336
		k_1 (min^{-1})	0.0006	0.0008	0.0006	0.0071	0.0006	0.0057
		R^2	0.963	0.850	0.664	0.660	0.989	0.974
		R_{adj}^2	0.959	0.831	0.622	0.618	0.988	0.971
		RMSE	0.134	0.185	0.259	0.481	0.044	0.130
	pseudo-second-order kinetic model	q_e (mg/g)	2.187	1.529	1.413	2.528	1.274	2.525
		k_2 (g/mg·min)	0.0322	0.0226	0.0357	0.0586	0.1123	0.0310
		R^2	0.992	0.982	0.996	0.999	0.997	1.000
		R_{adj}^2	0.991	0.980	0.995	0.999	0.997	1.000
		RMSE	0.062	0.064	0.028	0.022	0.021	0.014
	intraparticle diffusion	k_i (mg/g·$min^{0.5}$)	0.0207	0.0227	0.0145	0.0083	0.0067	0.0177
		C_i (mg/g)	1.576	0.911	0.975	2.119	1.030	1.923
		R^2	0.981	0.978	0.782	0.470	0.984	0.769
		R^2_{adj}	0.979	0.976	0.755	0.404	0.982	0.740
		RMSE	0.609	0.355	0.279	0.600	0.291	0.546

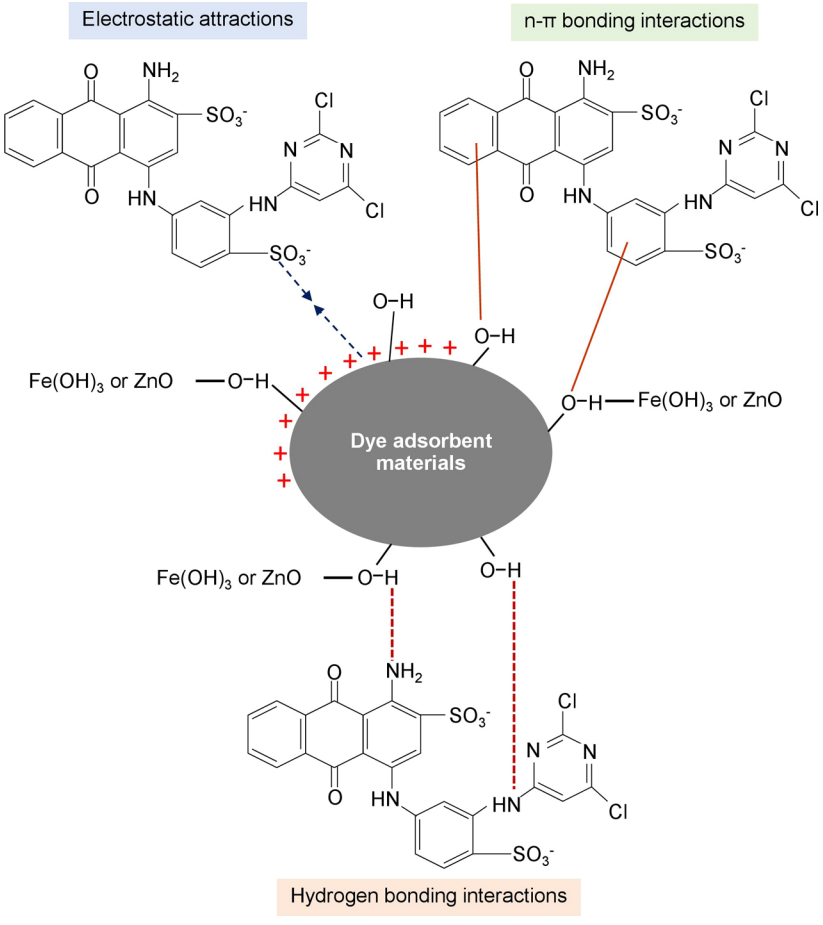

Figure 9. Schematic diagram of the possible mechanism of RB4 dye adsorption by dye adsorbent materials.

https://doi.org/10.1021/acsomega.2c03250
ACS Omega 2022, 7, 34839−34857

sodium hydroxide (NaOH) (RCI Labscan, Thailand), and zinc oxide (ZnO) (QRe¨C, New Zealand) were used. Sodium alginate ($NaC_6H_7O_6$) (Merck, Germany) and calcium chloride ($CaCl_2$) (Kemaus, New Zealand) were used for bead formation. The chemical structure of reactive blue 4 (RB4) dye ($C_{23}H_{14}Cl_2N_6O_8S_2$) (Sigma-Aldrich, Germany) is showed in Figure 10 and was used for preparing synthetic dye solution.

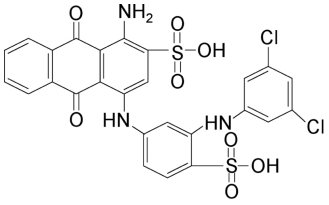

Figure 10. Chemical structure of RB4.

For the point of zero charge, 0.1 M hydrochloric acid (HCl) (RCI Labscan, Thailand) and 0.1 M sodium chloride (NaCl) (RCI Labscan, Thailand) were used. Finally, 0.5% nitric acid (HNO_3) (Merck, Germany) and 0.5% NaOH (RCI Labscan, Thailand) were used for pH adjustments.

4.4. Preparation of the Dye Solution. The dye solution was prepared from the stock solution of reactive blue 4 (RB4) dye of 100 mg/L concentration. It was prepared by adding 0.1 g of RB4 to a 100 mL beaker which contained 50 mL of deionized (DI) water, and then, it was mixed using a glass rod. The sample was poured into a 1000 mL volumetric flask, and then, approximately 950 mL of DI water was added until a volume of 1000 mL was obtained.

4.5. Material Synthesis. Figure 11 demonstrates the synthesis of all dye adsorbent materials, and the details were clearly explained below:

4.5.1. Synthesis of Bagasse or Bagasse Fly Ash Beads (BB or BFB). A total of 10 g of BP or BFP was added to a 1000 mL beaker containing 400 mL of 2% sodium alginate, and it was heated using a hot plate (Ingenieurbüro CAT M. Zipperer GmbH, M 6, Germany) at 60 °C with a stable stirring speed of 200 rpm. Then, the sample was added drop by drop to a 500 mL beaker containing 250 mL of 0.1 M $CaCl_2$ using a syringe with a needle (1.2 mm × 40 mm), and they were soaked in 0.1 M $CaCl_2$ solution for 24 h. After that, they were filtered, rinsed with DI water, and air-dried at room temperature for 12 h. The samples were kept in a desiccator before use called bagasse beads (BB) or bagasse fly ash beads (BFB).

4.5.2. Synthesis of Bagasse or Bagasse Fly Ash Beads with Mixed Iron(III) Oxide-Hydroxide (BBF or BFBF). A total of 10 g of BP or BFP was added to a 500 mL Erlenmeyer flask containing 160 mL of 5% $FeCl_3{\cdot}6H_2O$, and it was mixed using an orbital shaker (GFL, 3020, Germany) at 200 rpm for 3 h. Then, the sample was filtered and air-dried at room temperature for 12 h. After that, the sample was added to a 500 mL Erlenmeyer flask containing 160 mL of 5% NaOH, and it was shaken using an orbital shaker (GFL, 3020, Germany) at 200 rpm for 1 h. Then, it was filtered and air-dried at room temperature for 12 h and kept in a desiccator before use, called bagasse powder with mixed iron(III) oxide-hydroxide (BPF) or bagasse fly ash powder with mixed iron(III) oxide-hydroxide (BFPF). Then, BPF or BFPF was added to a 1000 mL beaker containing 400 mL of 2% sodium alginate, and then, it was homogeneously mixed and heated using a hot plate (Ingenieurbüro CAT M. Zipperer GmbH, M 6, Germany) at 60 °C with a constant stirring of 200 rpm. Then, the sample was added drop by drop using a 10 mL syringe with a needle size of 1.2 × 40 mm to 250 mL of 0.1 M $CaCl_2$. The beaded samples were soaked in 0.1 M $CaCl_2$ for 24 h, and then, they were filtered and rinsed with DI water. After that, they were air-dried at room temperature for 12 h and kept in a desiccator before use, called bagasse beads with mixed iron(III) oxide-hydroxide (BBF) or bagasse fly ash beads with mixed iron(III) oxide-hydroxide (BFBF).

4.5.3. Synthesis of Bagasse or Bagasse Fly Ash Beads with Mixed Zinc Oxide (BBZ or BFBZ). A total of 10 g of BP or BFP was added to a 500 mL Erlenmeyer flask containing 160 mL of 5% zinc oxide, and it was mixed using an orbital shaker (GFL, 3020, Germany) at 200 rpm for 3 h. Then, the sample was filtered and air-dried at 12 h, and it was kept in a desiccator, called bagasse powder with mixed zinc oxide (BPZ) or bagasse fly ash powder with mixed zinc oxide (BFPZ). Next, BPZ or BFPZ was added to a 1000 mL beaker containing 400 mL of 2% sodium alginate, and then, it was homogeneously mixed and heated using a hot plate (Ingenieurbüro CAT M. Zipperer GmbH, M 6, Germany) at 60 °C with constant stirring at 200 rpm. Then, the sample was added drop by drop using a 10 mL syringe with a needle size of 1.2 × 40 mm to 250 mL of 0.1 M $CaCl_2$. The beaded samples were soaked in 0.1 M $CaCl_2$ for 24 h, and then, they were filtered and rinsed with DI water. After that, they were air-dried at room temperature for 12 h and kept in a desiccator before use, called bagasse beads with mixed zinc oxide (BBZ) or bagasse fly ash beads with mixed zinc oxide (BFBZ).

4.6. Characterization of Dye Adsorbent Materials. Various characterization techniques such as X-ray diffractometry (XRD) (Bruker, D8 Advance, Switzerland) in a range of 2θ = 5−80°, field emission scanning electron microscopy with focused ion beam (FESEM-FIB) with energy dispersive X-ray spectrometry (EDX) (FEI, Helios NanoLab G3 CX), and Fourier transform infrared spectroscopy (FTIR) (Bruker, TENSOR 27, Hong Kong) in a range of 4000−600 cm^{-1} were used to determine the crystallized structures, surface morphologies, chemical compositions, and chemical functional groups of all dye adsorbent materials.

4.7. Batch Experiments. Dye removal efficiencies of dye adsorbent materials by varying the dosage, contact time, temperature, pH, and concentration were investigated through a series of batch experiments. The dye concentrations of all samples were analyzed using UV−VIS spectrophotometry (Hitachi, UH5300, Japan), and the details of batch experiments were clearly explained below.

4.7.1. Effect of Dosage. Different doses of dye adsorbent materials from 0.5 to 3.0 g were used to investigate the dye removal efficiencies with the control conditions of a sample volume of 100 mL, a dye concentration of 50 mg/L, a shaking speed of 150 rpm, a contact time for 12 h, a temperature of 50 °C, and pH 7. The lowest material dose with the highest dye removal efficiency was preferred as the optimum dose and used for the next experiment of the contact time effect.

4.7.2. Effect of Contact Time. The optimum dose from 4.7.1 and the contact time from 3 to 18 h were used to study the dye removal efficiencies of dye adsorbent materials with the contact time effect. The control conditions included a sample volume of 100 mL, a dye concentration of 50 mg/L, a shaking speed of 150 rpm, a temperature of 50 °C, and pH 7. The lowest contact time with the highest dye removal efficiency was

https://doi.org/10.1021/acsomega.2c03250
ACS Omega 2022, 7, 34839−34857

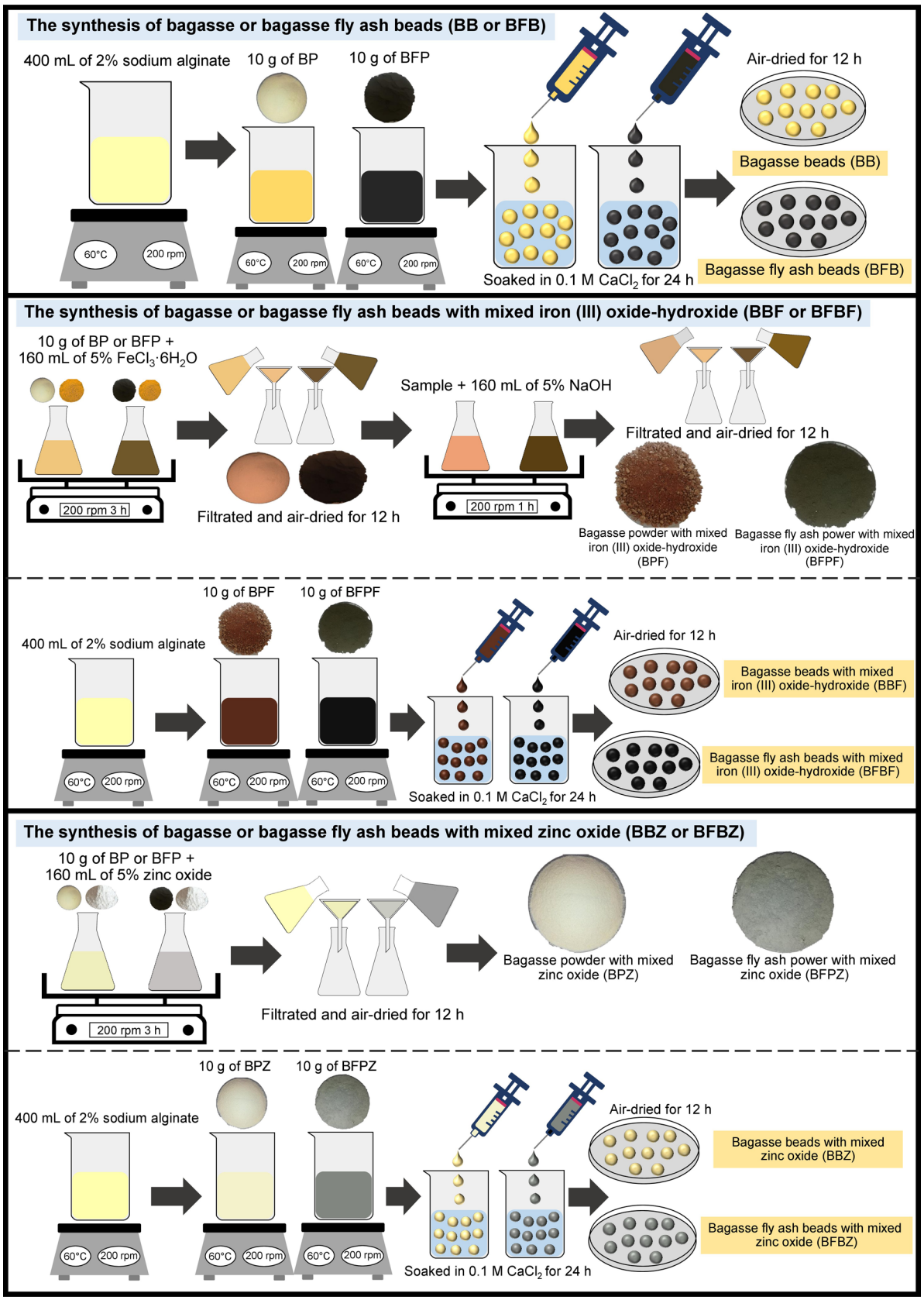

Figure 11. Synthesis of bagasse beads (BB), bagasse fly ash beads (BFB), bagasse beads with mixed iron(III) oxide-hydroxide (BBF), bagasse fly ash beads with mixed iron(III) oxide-hydroxide (BFBF), bagasse beads with mixed zinc oxide (BBZ), and bagasse fly ash beads with mixed zinc oxide (BFBZ).

https://doi.org/10.1021/acsomega.2c03250
ACS Omega 2022, 7, 34839−34857

preferred as the optimum contact time and used for the next experiment of the temperature effect.

4.7.3. Effect of Temperature. Different temperatures of 30−80 °C were used to examine the dye removal efficiencies of dye adsorbent materials with the control conditions including a sample volume of 100 mL, a dye concentration of 50 mg/L, a shaking speed of 150 rpm, pH 7, and the optimum dose and contact time from 4.7.1 and 4.7.2. The temperature with the highest dye removal efficiency was preferred as the optimum temperature and used for the next experiment of the pH effect.

4.7.4. Effect of pH. The optimum dose, contact time, and temperature from 4.7.1, 4.7.2, and 4.7.3 and pH of 3, 5, 7, 9, and 11 as representative acid, neutral, and base conditions were used to investigate the dye removal efficiencies of dye adsorbent materials with the pH effect. The control conditions included a sample volume of 100 mL, a dye concentration of 50 mg/L, and a shaking speed of 150 rpm. The pH value with the highest dye removal efficiency was preferred as the optimum pH and used for the next experiment of the concentration effect.

4.7.5. Effect of Concentration. Different concentrations of 30−90 mg/L were used to study the dye removal efficiencies of dye adsorbent materials with the control conditions including a sample volume of 100 mL, a shaking speed of 150 rpm, and the optimum dose, contact time, temperature, and pH from 4.7.1, 4.7.2, 4.7.3, and 4.7.4. The concentration with the highest dye removal efficiency was preferred as the optimum concentration.

To confirm the results, triplicate experiments were conducted, and the average values were reported. The dye removal efficiency in the percentage is calculated using the following eq 1

$$\text{dye removal efficiency (\%)} = ((C_0 - C_e)/C_0) \times 100 \quad (1)$$

where C_e is the equilibrium of dye concentration (mg/L) and C_0 is the initial dye concentration (mg/L).

4.8. Point of Zero Charge. A total of 0.1 M NaCl was used as the sample solution, and pH was adjusted from 2 to 12 using 0.1 M HCl and 0.1 M NaOH. Then, 0.1 g of each dye adsorbent material was added to 250 mL Erlenmeyer flasks containing 50 mL of 0.1 M NaCl with pH values of 2−12, and they were mixed using an orbital shaker (GFL, 3020, Germany) at room temperature at 150 rpm for 24 h. After that, the samples were characterized for the final pH value using a pH meter (Mettler Toledo,SevenGo with InLab 413/IP67, Switzerland), and ΔpH was calculated ($pH_{final} - pH_{initial}$). The value of the point of zero charge (pH_{pzc}) is a point which is the crossing line of ΔpH versus $pH_{initial}$ equal to zero.

4.9. Adsorption Isotherms. The adsorption pattern of dye adsorbent materials was explained using linear and nonlinear Langmuir, Freundlich, and Temkin isotherms following eqs 2−7 [61−63]

Langmuir isotherm

$$\text{linear: } C_e/q_e = 1/q_m K_L + C_e/q_m \quad (2)$$

$$\text{nonlinear: } q_e = q_m K_L C_e/1 + K_L C_e \quad (3)$$

Freundlich isotherm

$$\text{linear: } \log q_e = \log K_F + 1/n \log C_e \quad (4)$$

$$\text{nonlinear: } q_e = K_F C_e^{1/n} \quad (5)$$

Temkin isotherm

$$\text{linear: } q_e = RT/b_T \ln A_T + RT/b_T \ln C_e \quad (6)$$

$$\text{nonlinear: } q_e = RT/b_T \ln A_T C_e \quad (7)$$

where q_e is the capacity of dye adsorption on dye adsorbent materials at equilibrium (mg/g), q_m is the maximum amount of dye adsorption on dye adsorbent materials (mg/g), C_e is the equilibrium of dye concentration (mg/L), K_L is the Langmuir adsorption constant (L/mg), K_F is the Freundlich constant of adsorption capacity $(mg/g)(L/mg)^{1/n}$, n is the constant depicting the adsorption intensity, R is the universal gas constant (8.314 J/mol K), T is the absolute temperature (K), b_T is the constant related to the heat of adsorption (J/mol), and A_T is the equilibrium binding constant corresponding to maximum binding energy (L/g).[21] Graphs of linear Langmuir, Freundlich, and Temkin isotherms were plotted by C_e/q_e versus C_e, $\log q_e$ versus $\log C_e$, and q_e versus $\ln C_e$, respectively, whereas graphs of their nonlinear counterparts were plotted by q_e versus C_e.

For the adsorption isotherm experiment, the optimum dose of the dye adsorbent materials was applied with varying dye concentrations from 30 to 90 mg/L with the control conditions including a water sample of 100 mL, a contact time of 12 h, a temperature of 50 °C, pH 7, and a shaking speed of 150 rpm.

4.10. Adsorption Kinetics. The adsorption kinetics was investigated for explaining the adsorption rate and mechanism of dye adsorbent materials using linear and nonlinear pseudo-first-order, pseudo-second-order, and intraparticle diffusion models following eqs 8−12 [64−66]

Pseudo-first-order kinetic model

$$\text{linear: } \ln(q_e - q_t) = \ln q_e - k_1 t \quad (8)$$

$$\text{nonlinear: } q_t = q_e(1 - e^{-k_1 t}) \quad (9)$$

Pseudo-second-order kinetic model

$$\text{linear: } t/q_t = 1/k_2 q_e^2 + (1/q_e)t \quad (10)$$

$$\text{nonlinear: } q_t = k_2 q_e^2 t/(1 + q_e k_2 t) \quad (11)$$

Intraparticle diffusion model

$$\text{linear and nonlinear: } q_t = k_i t^{0.5} + C_i \quad (12)$$

where q_e (mg/g) and q_t (mg/g) are the capacities of the dye adsorbed by dye adsorbent materials at equilibrium and at the time (t), respectively, k_1 (min^{-1}), k_2 (g/mg·min), and k_i (mg/g·$min^{0.5}$) are the reaction rate constants of pseudo-first-order, pseudo-second-order, and intraparticle diffusion models, respectively, and C_i (mg/g) is the constant that gives an idea about the thickness of the boundary layer.[21] Graphs of linear pseudo-first-order, pseudo-second-order, and intraparticle diffusion models were plotted by $\ln(q_e - q_t)$ versus time (t), t/q_t versus time (t), and q_t versus time ($t^{0.5}$), respectively, whereas their nonlinear graphs were plotted by the capacity of the dye adsorbed by dye adsorbent materials at the time (q_t) versus time (t).

For the adsorption kinetic experiment, the optimum dose of the dye adsorbent materials was applied with the control conditions including a dye concentration of 50 mg/L, a sample volume of 1000 mL, a contact time for 15 h, a temperature of 50 °C, pH 7, and a shaking speed of 150 rpm.

https://doi.org/10.1021/acsomega.2c03250
ACS Omega 2022, 7, 34839−34857

AUTHOR INFORMATION

Corresponding Author

Pornsawai Praipipat − *Department of Environmental Science, Khon Kaen University, Khon Kaen 40002, Thailand; Environmental Applications of Recycled and Natural Materials (EARN) Laboratory, Khon Kaen University, Khon Kaen 40002, Thailand;* orcid.org/0000-0003-1311-2071; Email: pornprai@kku.ac.th; Fax: +66818774991

Authors

Pimploy Ngamsurach − *Department of Environmental Science, Khon Kaen University, Khon Kaen 40002, Thailand; Environmental Applications of Recycled and Natural Materials (EARN) Laboratory, Khon Kaen University, Khon Kaen 40002, Thailand*

Sutita Nemkhuntod − *Department of Environmental Science, Khon Kaen University, Khon Kaen 40002, Thailand*

Pakdiporn Chanaphan − *Department of Environmental Science, Khon Kaen University, Khon Kaen 40002, Thailand*

Complete contact information is available at: https://pubs.acs.org/10.1021/acsomega.2c03250

Author Contributions

P.N.: visualization and writing—original draft. S.N.: investigation. Pakdiporn Chanaphan: investigation. P.P.: supervision, conceptualization, funding acquisition, investigation, methodology, validation, visualization, writing—original draft, and writing—review and editing.

Notes

The authors declare no competing financial interest.

The raw/processed data required to reproduce these findings cannot be shared at this time due to legal or ethical reasons.

The raw/processed data required to reproduce these findings cannot be shared at this time, as the data also form part of an ongoing study.

The authors declare that they have no known competing financial interests or personal relationships that could have appeared to influence the work reported in this paper.

ACKNOWLEDGMENTS

The authors are grateful for the financial support from the Office of the Higher Education Commission and the Thailand Research Fund grant (MRG6080114), Coordinating Center for Thai Government Science and Technology Scholarship Students (CSTS), National Science and Technology Development Agency (NSTDA) Fund grant (SCHNR2016-122), and the Research and Technology Transfer Affairs of Khon Kaen University.

REFERENCES

(1) Lellis, B.; Fávaro-Polonio, C. Z.; Pamphile, J. A.; Polonio, J. C. Effects of Textile Dyes on Health and the Environment and Bioremediation Potential of Living Organisms. *Biotechnol. Res. Innov.* **2019**, *3*, 275−290.

(2) Benkhaya, S.; M'rabet, S.; El Harfi, A. A Review on Classifications, Recent Synthesis and Applications of Textile Dyes. *Inorg. Chem. Commun.* **2020**, *115*, No. 107891.

(3) Kishor, R.; Purchase, D.; Saratale, G. D.; Saratale, R. G.; Ferreira, L. F. R.; Bilal, M.; Chandra, R.; Bharagava, R. N. Ecotoxicological and Health Concerns of Persistent Coloring Pollutants of Textile Industry Wastewater and Treatment Approaches for Environmental Safety. *J. Environ. Chem. Eng.* **2021**, *9*, No. 105012.

(4) Katheresan, V.; Kansedo, J.; Lau, S. Y. Efficiency of Various Recent Wastewater Dye Removal Methods: A Review. *J. Environ. Chem. Eng.* **2018**, *6*, 4676−4697.

(5) Omo-Okoro, P. N.; Daso, A. P.; Okonkwo, J. O. A Review of the Application of Agricultural Wastes as Precursor Materials for the Adsorption of Per- and Polyfluoroalkyl Substances: A Focus on Current Approaches and Methodologies. *Environ. Technol. Innov.* **2018**, *9*, 100−114.

(6) Teixeira, R. A.; Lima, E. C.; Benetti, A. D.; Thue, P. S.; Cunha, M. R.; Cimirro, N. F. G. M.; Sher, F.; Dehghani, M. H.; dos Reis, G. S.; Dotto, G. L. Preparation of Hybrids of Wood Sawdust with 3-Aminopropyl-Triethoxysilane. Application as an Adsorbent to Remove Reactive Blue 4 Dye from Wastewater Effluents. *J. Taiwan Inst. Chem. Eng.* **2021**, *125*, 141−152.

(7) Aljeboree, A. M.; Alshirifi, A. N.; Alkaim, A. F. Kinetics and Equilibrium Study for the Adsorption of Textile Dyes on Coconut Shell Activated Carbon. *Arab. J. Chem.* **2017**, *10*, S3381−S3393.

(8) Bouhadjra, K.; Lemlikchi, W.; Ferhati, A.; Mignard, S. Enhancing Removal Efficiency of Anionic Dye (Cibacron Blue) Using Waste Potato Peels Powder. *Sci. Rep.* **2021**, *11*, No. 2090.

(9) Ahmed, A. E.; Majewska-Nowak, K. Removal of Reactive Dye from Aqueous Solutions Using Banana Peel and Sugarcane Bagasse as Biosorbents. *Environ. Prot. Eng.* **2020**, *46*, 121−135.

(10) Chowdhury, S.; Saha, T. K. Adsorption of Reactive Blue 4 (RB4) onto Rice Husk in Aqueous Solution. *Int. J. Sci. Eng. Res.* **2016**, *7*, 7−12.

(11) Abdelghaffar, F.; Abdelghaffar, R. A.; Mahmoud, S. A.; Youssef, B. M. Modified Sugarcane Bagasse for the Removal of Anionic Dyes from Aqueous Solution. *Pigm. Resin Technol.* **2019**, *48*, 464−471.

(12) Tahir, H.; Sultan, M.; Akhtar, N.; Hameed, U.; Abid, T. Application of Natural and Modified Sugar Cane Bagasse for the Removal of Dye from Aqueous Solution. *J. Saudi Chem. Soc.* **2016**, *20*, S115−S121.

(13) Mall, I. D.; Srivastava, V. C.; Agarwal, N. K. Removal of Orange-G and Methyl Violet Dyes by Adsorption onto Bagasse Fly Ash-Kinetic Study and Equilibrium Isotherm Analyses. *Dyes Pigm.* **2006**, *69*, 210−223.

(14) Sharma, M.; Bajpai, A. Superabsorbent Nanocomposite from Sugarcane Bagasse, Chitin and Clay: Synthesis, Characterization and Swelling Behaviour. *Carbohydr. Polym.* **2018**, *193*, 281−288.

(15) Nayeri, D.; Mousavi, S. A. Dye Removal from Water and Wastewater by Nanosized Metal Oxides-Modified Activated Carbon: A Review on Recent Researches. *J. Environ. Health Sci. Eng.* **2020**, *18*, 1671−1689.

(16) Pereira Da Silva, C.; Da Guarda Souza, M. O.; Dos Santos, W. N. L.; Oliveira Bastos Silva, L. Optimization of the Production Parameters of Composites from Sugarcane Bagasse and Iron Salts for Use in Dye Adsorption. *Sci. World J.* **2019**, *2019*, No. 8173429.

(17) Jiang, W.; Zhang, L.; Guo, X.; Yang, M.; Lu, Y.; Wang, Y.; Zheng, Y.; Wei, G. Adsorption of Cationic Dye from Water Using an Iron Oxide/Activated Carbon Magnetic Composites Prepared from Sugarcane Bagasse by Microwave Method. *Environ. Technol.* **2021**, *42*, 337−350.

(18) Zhang, F.; Chen, X.; Wu, F.; Ji, Y. High Adsorption Capability and Selectivity of ZnO Nanoparticles for Dye Removal. *Colloids Surf., A* **2016**, *509*, 474−483.

(19) Kaur, Y.; Jasrotia, T.; Kumar, R.; Chaudhary, G. R.; Chaudhary, S. Adsorptive Removal of Eriochrome Black T (EBT) Dye by Using Surface Active Low Cost Zinc Oxide Nanoparticles: A Comparative Overview. *Chemosphere* **2021**, *278*, No. 130366.

(20) Moosavi, S.; Lai, C. W.; Gan, S.; Zamiri, G.; Akbarzadeh Pivehzhani, O.; Johan, M. R. Application of Efficient Magnetic Particles and Activated Carbon for Dye Removal from Wastewater. *ACS Omega* **2020**, *5*, 20684−20697.

(21) Threepanich, A.; Praipipat, P. Powdered and Beaded Lemon Peels-Doped Iron (III) Oxide-Hydroxide Materials for Lead Removal Applications: Synthesis, Characterizations, and Lead Adsorption Studies. *J. Environ. Chem. Eng.* **2021**, *9*, No. 106007.

(22) Threepanich, A.; Praipipat, P. Efficacy Study of Recycling Materials by Lemon Peels as Novel Lead Adsorbents with Comparing of Material Form Effects and Possibility of Continuous Flow Experiment. *Environ. Sci. Pollut. Res.* **2022**, *29*, 46077−46090.
(23) Bahadur, N.; Das, P.; Bhargava, N. Improving Energy Efficiency and Economic Feasibility of Photocatalytic Treatment of Synthetic and Real Textile Wastewater Using Bagasse Fly Ash Modified TiO_2. *Chem. Eng. J. Adv.* **2020**, *2*, No. 100012.
(24) Lakouraj, M. M.; Mojerlou, F.; Zare, E. N. Nanogel and Superparamagnetic Nanocomposite Based on Sodium Alginate for Sorption of Heavy Metal Ions. *Carbohydr. Polym.* **2014**, *106*, 34−41.
(25) Huang, Y.; Gao, Y.; Zhang, Q.; Zhang, Y.; Cao, J. ji.; Ho, W.; Lee, S. C. Biocompatible FeOOH-Carbon Quantum Dots Nanocomposites for Gaseous NO_x Removal under Visible Light: Improved Charge Separation and High Selectivity. *J. Hazard. Mater.* **2018**, *354*, 54−62.
(26) Anbuvannan, M.; Ramesh, M.; Viruthagiri, G.; Shanmugam, N.; Kannadasan, N. Synthesis, Characterization and Photocatalytic Activity of ZnO Nanoparticles Prepared by Biological Method. *Spectrochim. Acta, Part A* **2015**, *143*, 304−308.
(27) El-Sherif, I. Y.; Fathy, N. A. Modification of Adsorptive Properties of Bagasse Fly Ash for Uptaking Cadmium from Aqueous Solution. *Environ. Res. Eng. Manage.* **2013**, *64*, 19−28.
(28) Mothé, C. G.; De Miranda, I. C. Characterization of Sugarcane and Coconut Fibers by Thermal Analysis and FTIR. *J. Therm. Anal. Calorim.* **2009**, *97*, 661−665.
(29) Ali, I.; Al-Othman, Z. A.; Alwarthan, A.; Asim, M.; Khan, T. A. Removal of Arsenic Species from Water by Batch and Column Operations on Bagasse Fly Ash. *Environ. Sci. Pollut. Res.* **2014**, *21*, 3218−3229.
(30) Sundarrajan, P.; Eswaran, P.; Marimuthu, A.; Subhadra, L. B.; Kannaiyan, P. One Pot Synthesis and Characterization of Alginate Stabilized Semiconductor Nanoparticles. *Bull. Korean Chem. Soc.* **2012**, *33*, 3218−3224.
(31) Ahmad, S.; Wong, Y. C.; Veloo, K. V. Sugarcane Bagasse Powder as Biosorbent for Reactive Red 120 Removals from Aqueous Solution. *IOP Conf. Ser.: Earth Environ. Sci.* **2018**, *140*, No. 01202.
(32) Said, A. E.-A. A.; Aly, A. A. M.; El-Wahab, M. M. A.; Soliman, S. A.; El-Hafez, A. A. A.; Helmey, V.; Goda, M. N. Application of Modified Bagasse as a Biosorbent for Reactive Dyes Removal from Industrial Wastewater. *J. Water Resour. Prot.* **2013**, *5*, 10−17.
(33) Sirajudheen, P.; Karthikeyan, P.; Vigneshwaran, S.; Meenakshi, S. Synthesis and Characterization of La(III) Supported Carboxymethylcellulose-Clay Composite for Toxic Dyes Removal: Evaluation of Adsorption Kinetics, Isotherms and Thermodynamics. *Int. J. Biol. Macromol.* **2020**, *161*, 1117−1126.
(34) Sposito, G. On Points of Zero Charge. *Environ. Sci. Technol.* **1998**, *32*, 2815−2819.
(35) Ibrahim, S. M.; Naghmash, M. A.; El-Molla, S. A. Synthesis and Application of Nano-Hematite on the Removal of Carcinogenic Textile Remazol Red Dye from Aqueous Solution. *Desalin. Water Treat.* **2020**, *180*, 370−386.
(36) Khapre, M.; Shekhawat, A.; Saravanan, D.; Pandey, S.; Jugade, R. Mesoporous Fe-Al-Doped Cellulose for the Efficient Removal of Reactive Dyes. *Mater. Adv.* **2022**, *3*, 3278−3285.
(37) Buthiyappan, A.; Gopalan, J.; Abdul Raman, A. A. Synthesis of Iron Oxides Impregnated Green Adsorbent from Sugarcane Bagasse: Characterization and Evaluation of Adsorption Efficiency. *J. Environ. Manage.* **2019**, *249*, No. 109323.
(38) Razali, S. Z.; Aziz, M. Y.; Edinur, H. A.; Razali Ishak, A. Adsorption of Methylene Blue onto Iron Oxide Magnetic Nanoparticles Coated with Sugarcane Bagasse. *IOP Conf. Ser.: Earth Environ. Sci.* **2020**, *596*, No. 012052.
(39) Galan, J.; Trilleras, J.; Zapata, P. A.; Arana, V. A.; Grande-Tovar, C. D. Optimization of Chitosan Glutaraldehyde-Crosslinked Beads for Reactive Blue 4 Anionic Dye Removal Using a Surface Response Methodology. *Life* **2021**, *11*, 1−20.
(40) Saadi, R.; Saadi, Z.; Fazaeli, R.; Fard, N. E. Monolayer and Multilayer Adsorption Isotherm Models for Sorption from Aqueous Media. *Korean J. Chem. Eng.* **2015**, *32*, 787−799.
(41) Ngamsurach, P.; Praipipat, P. Modified Alginate Beads with Ethanol Extraction of *Cratoxylum formosum* and *Polygonum odoratum* for Antibacterial Activities. *ACS Omega* **2021**, *6*, 32215−32230.
(42) Aguayo-Villarreal, I. A.; Ramírez-Montoya, L. A.; Hernández-Montoya, V.; Bonilla-Petriciolet, A.; Montes-Morán, M. A.; Ramírez-López, E. M. Sorption Mechanism of Anionic Dyes on Pecan Nut Shells (*Carya illinoinensis*) Using Batch and Continuous Systems. *Ind. Crops Prod.* **2013**, *48*, 89−97.
(43) Ullhyan, A. Adsorption of Reactive Blue-4 Dye from Aqueous Solution onto Acid Activated Mustard Stalk: Equilibrium and Kinetic Studies. *Glob. J. Biol. Agric. Health Sci.* **2014**, *3*, 98−105.
(44) Binupriya, A. R.; Sathishkumar, M.; Jung, S. H.; Song, S. H.; Yun, S. I. A Novel Method in Utilization of Bokbunja Seed Eastes from Wineries in Liquid-Phase Sequestration of Reactive Blue 4. *Int. J. Environ. Res.* **2009**, *3*, 1−12.
(45) Ibrahim, S.; Shuy, W. Z.; Ang, H.-M.; Wang, S. Preparation of Bioadsorbents for Effective Adsorption of a Reactive Dye in Aqueous Solution. *Asia-Pac. J. Chem. Eng.* **2009**, *7*, 743−753.
(46) Lawal, I. A.; Chetty, D.; Akpotu, S. O.; Moodley, B. Sorption of Congo Red and Reactive Blue on Biomass and Activated Carbon Derived from Biomass Modified by Ionic Liquid. *Environ. Nanotechnol., Monit. Manage.* **2017**, *8*, 83−91.
(47) Hong, G. B.; Wang, Y. K. Synthesis of Low-Cost Adsorbent from Rice Bran for the Removal of Reactive Dye Based on the Response Surface Methodology. *Appl. Surf. Sci.* **2017**, *423*, 800−809.
(48) Ma, C. M.; Hong, G. B.; Wang, Y. K. Performance Evaluation and Optimization of Dyes Removal Using Rice Bran-Based Magnetic Composite Adsorbent. *Materials* **2020**, *13*, 1−18.
(49) Binupriya, A. R.; Sathishkumar, M.; Ku, C. S.; Yun, S. I. Sequestration of Reactive Blue 4 by Free and Immobilized *Bacillus subtilis* Cells and Its Extracellular Polysaccharides. *Colloids Surf., B* **2010**, *76*, 179−185.
(50) Bagchi, M.; Ray, L. Adsorption Behavior of Reactive Blue 4, a Tri-Azine Dye on Dry Cells of *Rhizopus oryzae* in a Batch System. *Chem. Speciation Bioavailability* **2015**, *27*, 112−120.
(51) Sun, D.; Zhang, Z.; Wang, M.; Wu, Y. Adsorption of Reactive Dyes on Activated Carbon Developed from *Enteromorpha prolifera*. *Am. J. Anal. Chem.* **2013**, *4*, 17−26.
(52) Nascimento, M. A.; Cruz, J. C.; Rodrigues, G. D.; de Oliveira, A. F.; Lopes, R. P. Synthesis of Polymetallic Nanoparticles from Spent Lithium-Ion Batteries and Application in the Removal of Reactive Blue 4 Dye. *J. Cleaner Prod.* **2018**, *202*, 264−272.
(53) Pal, S.; Patra, A. S.; Ghorai, S.; Sarkar, A. K.; Mahato, V.; Sarkar, S.; Singh, R. P. Efficient and Rapid Adsorption Characteristics of Templating Modified Guar Gum and Silica Nanocomposite toward Removal of Toxic Reactive Blue and Congo Red Dyes. *Bioresour. Technol.* **2015**, *191*, 291−299.
(54) Rastgordani, M.; Zolgharnein, J. Simultaneous Determination and Optimization of Titan Yellow and Reactive Blue 4 Dyes Removal Using Chitosan@hydroxyapatite Nanocomposites. *J. Polym. Environ.* **2021**, *29*, 1789−1807.
(55) Karaer, H.; Kaya, I. Synthesis, Characterization of Magnetic Chitosan/Active Charcoal Composite and Using at the Adsorption of Methylene Blue and Reactive Blue4. *Microporous Mesoporous Mater.* **2016**, *232*, 26−38.
(56) Vakili, M.; Rafatullah, M.; Ibrahim, M. H.; Abdullah, A. Z.; Gholami, Z.; Salamatinia, B. Enhancing Reactive Blue 4 Adsorption through Chemical Modification of Chitosan with Hexadecylamine and 3-Aminopropyl Triethoxysilane. *J. Water Process Eng.* **2017**, *15*, 49−54.
(57) Gupta, V. K.; Nayak, A. Cadmium Removal and Recovery from Aqueous Solutions by Novel Adsorbents Prepared from Orange Peel and Fe_2O_3 Nanoparticles. *Chem. Eng. J.* **2012**, *180*, 81−90.
(58) Mohamed, N. B.; Ngadi, N.; Wong, S.; Yahya, N. Y.; Hassan, O.; Inuwa, I. M.; Opotu, L. A.; Ali, N. Facile Synthesis of Polyethylenimine-Modified Sugarcane Bagasse Adsorbent for Re-

https://doi.org/10.1021/acsomega.2c03250
ACS Omega 2022, 7, 34839−34857

moval of Anionic Dye in Aqueous Solution. *Sci. Afr.* **2022**, *16*, No. e01135.
(59) Ma, J.; Hou, L.; Li, P.; Zhang, S.; Zheng, X. Modified Fruit Pericarp as an Effective Biosorbent for Removing Azo Dye from Aqueous Solution: Study of Adsorption Properties and Mechanisms. *Environ. Eng. Res.* **2022**, *27*, No. 200634.
(60) Awasthi, A.; Arya, A.; Gupta, P.; Kumar, R.; Singh, J.; Datta, D. Adsorption of Reactive Blue-13, an Acidic Dye, from Aqueous Solution Using Magnetized Activated Carbon. *J. Chem. Eng. Data* **2020**, *65*, 2220−2229.
(61) Langmuir, I. The Adsorption of Gases on Plane Surfaces of Glass, Mica and Platinum. *J. Am. Chem. Soc.* **1918**, *40*, 1361−1403.
(62) Freundlich, H. Over the Adsorption in Solution. *J. Phys. Chem. A* **1906**, *57*, 385−470.
(63) Temkin, M. I.; Pyzhev, V. Kinetics of Ammonia Synthesis on Promoted Iron Catalysts. *Acta Physiochim. URSS* **1940**, *12*, 327−356.
(64) Lagergren, S. About the Theory of So-Called Adsorption of Soluble Substances. *Sven. Vetenskapsakad. Handingarl.* **1898**, *24*, 1−39.
(65) Ho, Y. S.; McKay, G. Pseudo-Second Order Model for Sorption Processes. *Process Biochem.* **1999**, *34*, 451−465.
(66) Weber, W. J.; Morris, J. C. Kinetics of Adsorption Carbon from Solution. *J. Sanit. Eng. Div.* **1963**, *89*, 31−60.

https://doi.org/10.1021/acsomega.2c03250
ACS Omega 2022, 7, 34839−34857